https://doi.org/10.5194/egusphere-2026-3122
Preprint. Discussion started: 11 June 2026
© Author(s) 2026. CC BY 4.0 License.

A Shifting Balance: Dynamic and Thermodynamic Controls on Arctic Sea Ice Thickness

Luisa von Albedyll[1], Robert Ricker[2], Frank Kauker[1], Daniel Krogmann[1], and Stefan Hendricks[1]

[1]Alfred-Wegener-Institut, Helmholtz-Zentrum für Polar- und Meeresforschung, Bremerhaven, Germany
[2]Observing Systems, NORCE Norwegian Research Centre, Tromsø, Norway

Correspondence: Luisa von Albedyll (luisa.von.albedyll@awi.de)

Abstract. Arctic sea ice thickness has declined rapidly over recent decades, yet the relative roles of thermodynamic growth and dynamic redistribution in driving this change remain poorly constrained at basin scale. We quantify thermodynamic and dynamic contributions to sea-ice thickness change together with their uncertainties across the Arctic from 2002 to 2020 by combining satellite-derived thickness with sea-ice model simulations (Icepack) along trajectories. Separating dynamical thickening (30%), dynamical thinning (-24%), and lead-ice growth (10.2%) shows that dynamic processes contribute nearly as much to the average winter ice growth of 0.21 m per month as thermodynamic processes (35.8%). Regional, seasonal, and thickness-dependent variability is consistent with large-scale dynamic patterns and the ice-growth feedback. We quantify the effects of the overly smooth deformation forcing, which leads to an underestimation of large dynamic events and a substantial noise floor during dynamically quiet periods, and relate their magnitude to other sources of uncertainty. Analyzing the long-term trend from 2002–2020, we resolve a weak increase in median sea ice deformation (1.5% per year) and net dynamic thickness change (12% per year) within the limits of our study setup. Overall, our results suggest that increasing deformation in the Arctic enhances net dynamic thickness change and acts as a negative feedback in the pan-Arctic winter thickness budget.

1 Introduction

The Arctic Ocean is transitioning from perennial sea ice coverage to summers without ice, accompanied by a significant reduction in average sea ice thickness by more than half in the past sixty years (e.g., Kwok, 2018; Bocquet et al., 2024). This thinning ice has various implications for the climate and ecosystem of the Arctic, making accurate climate models and predictions crucial. Interestingly, the rate of decline in thickness and volume has slowed since the 2010s (Kwok, 2018; Kacimi and Kwok, 2022), despite rising Arctic air and ocean temperatures (Polyakov et al., 2017; Rantanen et al., 2022). This raises questions about the internal variability (England et al., 2025) and feedback mechanisms at play that can either enhance or dampen sea ice thickness loss. Since these climate feedbacks differ between thermodynamic and dynamic thickness change, it is essential to quantify their respective contributions to sea ice thickness change separately.

Although several studies have investigated winter thermodynamic processes and their associated feedbacks (Petty et al., 2018; Stroeve et al., 2018; Cornish et al., 2022), the role of dynamics for the winter sea ice thickness remains less well understood. Regional studies suggest that dynamic processes significantly contribute (25-40%) to ice volume and mean thickness

https://doi.org/10.5194/egusphere-2026-3122
Preprint. Discussion started: 11 June 2026
© Author(s) 2026. CC BY 4.0 License.

during winter (Kwok, 2006; Kwok and Cunningham, 2016; Koo et al., 2021; von Albedyll et al., 2022). The few existing pan-Arctic studies indicate strong spatial variability in the dynamic contribution to ice volume change (Ricker et al., 2021; Anheuser et al., 2023; Heorton et al., 2025). For instance, Anheuser et al. (2023) found values ranging from -50% (-0.20 m per month) in the start regions of the Transpolar Drift to +33% (0.10 m per month) in the Canadian Arctic Archipelago. On a pan-Arctic scale, they found that dynamics contribute negatively to the growth of sea ice volume by around one quarter of the magnitude of thermodynamic growth (Anheuser et al., 2023).

However, the existing pan-Arctic studies summarize dynamic thickness change in one term despite their opposing effects on the ice thickness distribution, treat dynamics or thermodynamics only as the residuals of the other without providing explicit estimates with uncertainties, or are too short to observe a potential regime shift around the 2010s (Ricker et al., 2021; Anheuser et al., 2023; Heorton et al., 2025).

This research seeks to fill this gap by analyzing long-term regional and temporal trends in observed thickness change along Lagrangian sea ice trajectories, and by using the sea ice model Icepack (Hunke et al., 2018) to explicitly quantify contributions from thermodynamic growth of existing ice, dynamical thickening due to ridging, dynamical thinning due to open-water formation, and new ice growth in those leads. To achieve the most stable and robust results, our analysis is based on the long-term, stable climate data records of sea ice thickness (Hendricks et al., 2018a, b), concentration (OSI SAF, 2022b), and sea ice drift (OSI SAF, 2022a).

2 Datasets

2.1 Drift-Aware Sea-Ice Thickness product

The principal dataset utilized here is based on the Drift-Aware Sea-Ice Thickness (DA-SIT) product developed within the ESA Climate Change Initiative (CCI) (Ricker et al., 2025a). DA-SIT integrates sea ice thickness observations of ice parcels obtained from altimeters, alongside their Lagrangian drift trajectories derived from passive microwave (PMW) radiometers. DA-SIT is based on the CCI climate data record version 3.0 of SIT for the Northern Hemisphere polar region (Hendricks et al., 2018a, b), sea ice concentration (OSI SAF, 2022b), and sea ice drift (OSI SAF, 2022a). In the basic DA-SIT configuration, ice parcels are advected with a width of 10 km over a period of 15 days, both forwards and backwards in time. For this study, however, we use DA-SIT with an advection period covering the full winter season backwards in time (April to October of the previous year) and a parcel width of 75 km.

DA-SIT covers the growth seasons (1 October to 30 April) with observations from the radar altimeters Envisat (2002-2012) and CryoSat-2 (2010-2020). As an altimeter-based product, the actual derived quantity is sea ice freeboard that is converted to sea ice thickness assuming hydrostatic equilibrium and using auxiliary information on snow depth and snow and ice density. In addition to the mean thickness of each parcel and its trajectory, DA-SIT also provides (among other quantities) the uncertainties of the thickness measurements and of the trajectory location (drift uncertainty).

https://doi.org/10.5194/egusphere-2026-3122
Preprint. Discussion started: 11 June 2026
© Author(s) 2026. CC BY 4.0 License.

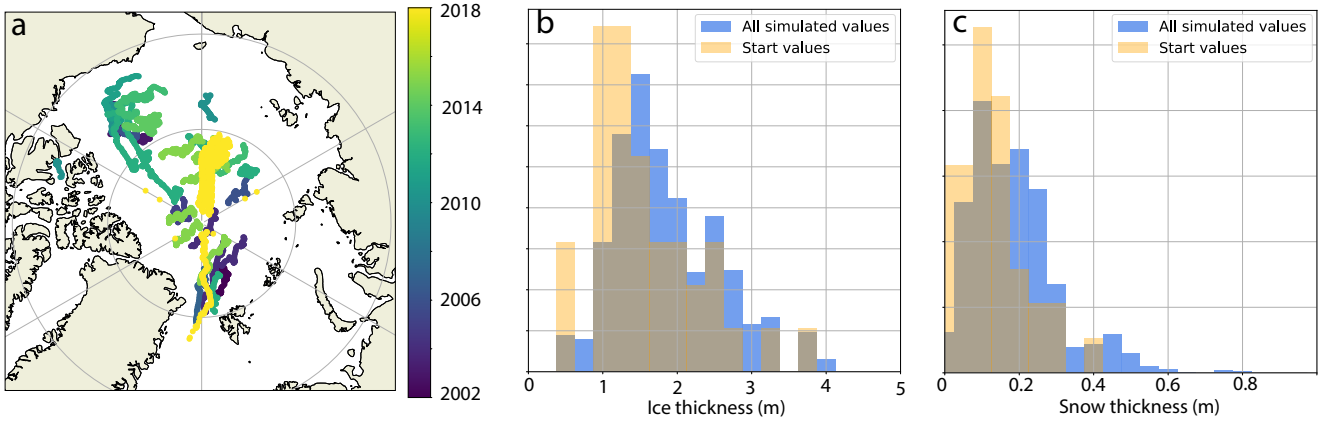


Figure 1. Overview of the IMB reference dataset. Panel a shows an Arctic map of the 38 IMB tracks. Colors indicate the year of the start of the drift. Panel b shows the thickness distributions at the beginning of the simulations (orange) and all simulated thickness values (blue). Panel c like panel b for snow thickness.

2.2 Sea ice deformation from RGPS

To evaluate sea ice deformation derived from the low-resolution sea ice drift along the trajectories of DA-SIT, we used the Radarsat Geophysical Processor System (RGPS) dataset. RGPS provides high-resolution sea ice deformation and trajectories from Synthetic Aperture Radar (SAR) imagery, particularly from the Radarsat-1 satellite. We have used a pre-processed subset overlapping our study period with data from January to March of the winters 2003-2008 (Bouchat and Hutter, 2022). It covers large parts of the Pacific Arctic with a spatial and temporal resolution of 10 km and 3 days.

2.3 Ice Mass Balance Buoys

For evaluation and quality control of Icepack's thermodynamic process formulations, we selected a reference dataset of Lagrangian sea ice thickness and snow depth observations from 38 Ice Mass Balance buoys (IMBs, Grosfeld et al., 2016; Preußer et al., 2025; Perovich et al., 2024). The 38 IMBs were selected because they had collected at least two months of data between October and April from 2002 to 2018, were not suspected to have experienced dynamic events and were a spatially representative subset of the Arctic Ocean (Figure 1). With initial ice (snow) thicknesses between 0.5–4 m (0–0.4 m) they also cover a representative fraction of the simulated DA-SIT trajectories (Figure 1b,c). The IMBs hosted on the Sea Ice Portal (https://data.seaiceportal.de/ Grosfeld et al., 2016) contain uncertainty estimates for each measurement point ranging between 4 and 8 cm depending on the retrieval method (Preußer et al., 2025). On average, the ice thickness measurement uncertainty was 5 cm. In the absence of any information for the IMBs hosted on the CRREL-Dartmouth Mass Balance Buoy Program (Perovich et al., 2024), we assume the same uncertainties.

https://doi.org/10.5194/egusphere-2026-3122
Preprint. Discussion started: 11 June 2026
© Author(s) 2026. CC BY 4.0 License.

3 Methods

We aim to derive sea ice thickness change along Lagrangian trajectories from the observational records (Section 3.1) and to use simulations of the column model Icepack (Hunke et al., 2018, modified version 1.1.0,) along these trajectories to split the total thickness change into contributions from thermodynamic growth of existing ice, dynamical thickening due to ridging, dynamical thinning due to open-water formation, and new ice growth in those leads (Section 3.3).

3.1 Sea ice thickness change along Lagrangian trajectories

We evaluate changes in sea ice thickness on a monthly time scale and a spatial scale of approximately $500\,\mathrm{km} \times 500\,\mathrm{km}$ (i.e. a circle with a radius of 250 km). These scales were selected to minimize uncertainty, particularly with regard to the spatial representation of the thickness and deformation of the sea ice. Section 4.3 and Appendix 7.2 provide more detailed information.

As pointed out in Section 2.1, we use a customized DA-SIT configuration that contains all trajectories of a winter season terminating on 30 April. We use these DA-SIT trajectories to derive changes in sea ice thickness through the following steps:

1. We define the starting points by selecting all the grid cells in the NSIDC Arctic Region Mask, with a spatial resolution of 75 km (Stewart and Meier, 2021), that are classified as sea ice in the climatology (T. Lavergne, MET Norway, pers. comm.) Around each starting point, we define a circle with a radius of 250 km and collect all trajectories from the DA-SIT file ending within this circle. This set of trajectories is meant to represent the "same" ice and is processed together in all subsequent operations.

2. A set of trajectories contains a variable amount of individual trajectories, each of which contains the averaged altimeter thickness retrieval of an ice parcel at a specific time between October 1 and April 30 and the time and location of the observed ice parcel between the measurement and April 30.

3. We derive a mean ice thickness distribution time series for a set of trajectories by averaging all sea ice thickness histograms from trajectories starting on the corresponding date. We only include dates where at least 200 individual altimeter observations are available for a particular date.

4. We derive a mean "center" trajectory of a set of trajectories by averaging all available location data at each timestep.

3.2 Deformation forcing along Lagrangian trajectories

To estimate the dynamic contribution to sea-ice thickness change, deformation estimates are required to force Icepack along the trajectories. Sea-ice deformation is derived from polygons constructed from the set of DA-SIT trajectories. To ensure high-quality estimates, polygons are defined with six vertices, acute angles smaller than 25° are excluded, and the selected vertices must be separated by at least 37.5 km (half the spatial resolution) to increase the independence of the drift vectors (e.g., Itkin et al., 2017). Green's theorem is then applied to sequential polygons to calculate daily deformation (e.g., Kwok et al., 2003, 2008; Hutchings et al., 2011; Dierking et al., 2020). For each day, we select the ten polygons enclosing the highest number

https://doi.org/10.5194/egusphere-2026-3122
Preprint. Discussion started: 11 June 2026
© Author(s) 2026. CC BY 4.0 License.

of individual trajectories and average their deformation estimates to obtain a daily mean. This maximizes the common spatial coverage of deformation and thickness observations. A detailed description of the polygon selection procedure is provided in Appendix 7.3. The spread of the ten estimates is used to quantify uncertainties of the deformation estimates (Section 4.3.2, *Uncertainty of the dynamic ice thickness change*).

Before using our sea ice deformation dataset derived from the PMW trajectories in DA-SIT to force the simulations, we compared it with high-resolution sea ice drift and deformation data derived from RGPS trajectories (Section 2.2). Specifically, we assessed the ability of our PMW deformation data to reproduce accumulated monthly deformation, the seasonal cycle, regional differences, and interannual variability. We applied the same deformation retrieval method to the RGPS trajectories as used for the DA-SIT trajectories. The detailed procedure for constructing trajectories and averaging deformation from RGPS is described in Appendix 7.4. Results of the evaluation are presented in Section 4.3.2 (*Uncertainty of the dynamic ice thickness change*).

3.3 Icepack simulations along Lagrangian trajectories

The "Icepack" vertical column physics package of sea ice and snow is maintained by the CICE Consortium (Hunke et al., 2018). The code includes several options for simulating sea ice thermodynamics, mechanical redistribution (ridging) and associated area and thickness changes. In addition, the model supports a number of tracers, including thickness, enthalpy, ice age, first-year ice area, deformed ice area and volume, melt ponds, and biogeochemistry. Icepack is implemented in the Los Alamos Sea Ice Model CICE (Hunke et al., 2020) as a git submodule. The purpose of Icepack is to provide the column physics model as a separate library for use in other host models such as CICE or standalone. The Icepack code is available from https://github.com/CICE-Consortium/Icepack.

The design of Icepack allows for flexible experimentation with sea-ice physics as a result of the implementation of various thermodynamic and dynamic parameterizations. In the standalone setup it requires thermodynamic (atmosphere and ocean) and dynamic forcing (opening and closing), which are here prescribed along the DA-SIT trajectories. Section 4.3.2 justifies the selected forcing datasets. Icepack is particularly suitable for our application because it can be applied in a Lagrangian framework and across different spatial scales. Since no grid cell size is specified, the effective spatial scale is determined by the resolution of the forcing datasets. The model is computationally efficient and straightforward to configure. Most importantly, Icepack resolves the interaction between thermodynamic and dynamic processes. In addition, Icepack/CICE forms the sea-ice component of many climate models, facilitating future comparisons between observational estimates and climate model output.

3.3.1 Icepack Thermodynamics

We use a customized version of Icepack based on version 1.1.0 (Hunke et al., 2018) with seven ice layers, forty equally distributed ice classes with 25 cm bin width, and one snow layer. The mushy-layer thermodynamics were updated following Plante et al. (2024) by applying the code modification introduced in GitHub commit 4c87095 (7 August 2024, [1]). This update introduces a new one-step scheme that corrects previously overestimated congelation ice growth rates, erroneous melt, and

[1] https://github.com/CICE-Consortium/Icepack/commit/4c87095256c1c599c3ccaa857a95744158751a60

https://doi.org/10.5194/egusphere-2026-3122
Preprint. Discussion started: 11 June 2026
© Author(s) 2026. CC BY 4.0 License.



excessive frazil ice formation. Following Plante et al. (2024), we tuned the one-step scheme by testing different values of ω (dSdt_slow_mode), which controls the strength of slow drainage, and ϕ_{init} (phi_i_mushy), the initial liquid fraction for slow drainage. Based on our tuning results (Appendix 7.1), we selected $\omega = -5.0 \times 10^{-8}$ m s^{-1} and $\phi_{init} = 0.85$. In addition, instead of prescribing a constant initial snow surface temperature, we initialize the ice temperature with the surface air temperature from the atmospheric forcing. Throughout this study, Icepack is run with mushy thermodynamics using the tuned one-step scheme.

For the ocean forcing we use output from the Finite volumE Sea Ice–Ocean Model (FESOM2, Danilov et al., 2017) in CORE2 resolution (Wang et al., 2014) driven by ERA atmospheric forcing. Along each center trajectory, we prescribe mixed-layer salinity, initial mixed-layer temperature, and ocean heat flux into the mixed layer as time- and location-dependent forcing. For the atmospheric forcing datasets, we evaluated the 6-hourly NCEP Climate Forecast System Reanalysis (CFSR; Saha et al., 2010) for 2002 to 2010 extended by NCEP's Climate Forecast System Version 2 (CFSv2, Saha et al., 2014) for 2011 to 2020 and the hourly ERA5 reanalysis (Hersbach et al., 2020). Icepack simulations without dynamics were performed along the trajectories of 38 IMBs (Section 2.3; 6330 daily observations, 5146 monthly differences) and compared with the IMBs' sea-ice thickness and snow depths. Monthly thickness changes were calculated by taking the difference in mean thickness 30 days apart. The monthly change has the advantage that uncertainties do not accumulate over the full lifespan of a simulation. Since it reflects well the quantity that we analyze in the course of this study, we base our decisions on this metric. The evaluation is presented in Section 4.3.2 (*Uncertainty of simulated thermodynamic thickness change*).

We observed that most buoy simulations exhibit rapid ice growth of 3–5 cm during the first 1–3 days, followed by 1–2 days of little growth. As this pattern is not evident in the IMB observations, we attribute it to model adjustment toward equilibrium between the snow and ice thickness, ocean temperature, and atmospheric forcing. To reduce this "cold-start" model bias, we replaced the thermodynamic growth rates during the first five days with the mean thermodynamic growth rate of days 6–10. The effectiveness of this correction was evaluated by comparing RMSE, MAD, and bias of the corrected time series with simulations that exclude the first 10 days. The correction reduces differences to a level comparable to or lower than those obtained when discarding the first 10 days. Thus, we were confident in applying this correction to the thermodynamic growth of all trajectories.

3.3.2 Icepack Dynamics

We updated the dynamics of our custom Icepack 1.1.0 configuration by applying the code modification introduced in GitHub commit e6727c1 (12 May 2023, [2]). This update substantially revises how dynamic forcing is treated in the ridging and closing routines. In the new "uniform ice" mode, ice entering the Icepack column during convergence is assumed to have the same ice thickness distribution, whereas in the original "open water" scheme the area created by ridging is filled with open water. In our Lagrangian framework, the properties of ice entering the column are not known a priori. We therefore implemented and benchmarked both schemes against the DA-SIT observations. Opening and closing rates are derived from divergence ($\dot{\epsilon}_I$),

[2]https://github.com/CICE-Consortium/Icepack/commit/e6727c13f1caef5fb8c79db46416cffb6c4668bf

https://doi.org/10.5194/egusphere-2026-3122
Preprint. Discussion started: 11 June 2026
© Author(s) 2026. CC BY 4.0 License.

convergence ($-\min(\dot{\epsilon}_I, 0)$), and shear ($\dot{\epsilon}_{II}$) following Lipscomb et al. (2007) and Ungermann and Losch (2018):

$$\Delta = \sqrt{\dot{\epsilon}_I^2 + \left(\frac{\dot{\epsilon}_{II}}{e}\right)^2}, \quad \text{shear}_{\text{rdg}} = \tfrac{1}{2}\left(\Delta - |\dot{\epsilon}_I|\right), \tag{1}$$

$$\text{opening} = \text{divergence} + C_s\,\text{shear}_{\text{rdg}}, \quad \text{closing} = \text{convergence} + C_s\,\text{shear}_{\text{rdg}}. \tag{2}$$

Here $e = 2$ is the ratio of the elliptical yield curve, and $C_s = 0.25$ is a tuning parameter controlling the fraction of shear deformation that contributes to lead opening and closing.

3.3.3 Thermodynamic and dynamic contributions from Icepack runs

Icepack is initialized with the DA-SIT ice thickness distribution and driven along the trajectory by ocean (SSS and deep ocean heat flux into the mixed layer), atmospheric (2 m temperature and humidity, 10 m wind speed, downward thermal and solar radiation, and rain- and snowfall) and deformation (opening and closing) forcing.

We simulate thickness change along the trajectories with two different Icepack runs: First, Icepack runs with dynamic forcing ("dynamics" run) and second, with dynamics turned off ("no dynamics" run). Next, we quantify and define the individual contributions to sea ice thickness from the two runs as follows:

1. **Thermodynamics**: Thermodynamic ice growth (excluding lead ice growth): This is quantified by the "no dynamics" run, specifically the output variable "ice_volume_involved_thermodynamics".
2. **Lead ice growth**: Dynamics-induced thermodynamic growth: This includes new ice formation in leads and their subsequent growth, as well as compensating effects such as reduced ice growth beneath ridges. It is calculated as the difference between the thermodynamic ice growth (1.) and the thermodynamic growth in the "dynamics" run, specifically the output variable "ice_volume_involved_thermodynamics".
3. **Dynamical thickening**: Convergence-induced thickening (ridging): This is quantified by positive changes in the variable "ice_volume_involved_dynamics" in the "dynamics" run.
4. **Dynamical thinning**: Divergence-induced thinning (open-water formation in leads): This is quantified by negative changes in the variable "ice_volume_involved_dynamics" in the "dynamics" run.

3.4 Quality control of observed and simulated trajectories and curated dataset

We applied a two-stage quality control procedure to all observed and modeled sea ice thickness trajectories. In stage 1, we excluded observed and simulated trajectories outside the physically plausible range of thickness change. For both DA-SIT and Icepack, months with thickness changes exceeding 1.6 m were removed, as well as trajectories with less than 0.3 m total thickness change over the entire season. To address orbit-pattern artifacts producing short-term variability in DA-SIT trajectories (see Section 4.3), we excluded months containing periods where detrended daily observations varied by more than 0.5 m within 10 days. On the Icepack side, the "uniform ice" mode can produce implausibly thick ice due to excessive ridging. We therefore excluded all subsequent trajectory points once the accumulated thickness contribution from ridging exceeded 0.8 m.

https://doi.org/10.5194/egusphere-2026-3122
Preprint. Discussion started: 11 June 2026
© Author(s) 2026. CC BY 4.0 License.

Sensitivity tests with different threshold values showed that the overall results were not sensitive to the exact choices. Further, we excluded time steps with travel distances exceeding 50 km, as these are physically implausible artifacts resulting from the averaging of the set of trajectories into a center trajectory.

In stage 2, we further restricted the dataset to a curated subset containing only values from DA-SIT–Icepack pairs with consistent monthly change rates. In detail, we compared monthly dynamic thickness change from Icepack (only the dynamic contributions) with dynamic thickness change of DA-SIT (DA-SIT$_{\mathrm{dyn}}$) which was estimated by subtracting the Icepack thermodynamic contribution from the total thickness of DA-SIT.

To verify that the filtering does not substantially alter the dataset characteristics, we compared the distributions of monthly thickness change in the original and curated datasets using the two-sample Kolmogorov–Smirnov (KS) statistic. Key results are also shown in the following for the non-curated dataset to demonstrate that the filtering does not introduce a significant bias.

Model-observation pair values were retained when the absolute difference between the monthly dynamic thickness changes from Icepack and DA-SIT remained within 90% of DA-SIT$_{\mathrm{dyn}}$. This proportional criterion ensures that disagreement between the two estimates remains small relative to the signal magnitude. For very small thickness changes, the tolerance was relaxed using

$$\mathrm{tol} = \sqrt{(0.1\,\mathrm{m})^2 + \left(0.9\,|\Delta h_{\mathrm{DA-SIT_{dyn}}}|\right)^2},$$

which introduces a baseline uncertainty of 0.1 m. For large thickness changes ($> |0.33|$ m), an additional upper bound of |0.3| m was imposed on the allowed difference between model and observations. Model-observation pairs exceeding either threshold were excluded.

Figure 2a shows the distribution of DA-SIT monthly thickness change for the full and curated datasets (pan-Arctic, all years). The two distributions closely overlap (Kolmogorov–Smirnov test, KS = 0.16), indicating that the curated dataset preserves the overall characteristics of the original distribution. The curated distribution is slightly narrower, reflecting a reduction of extreme thickness-change values, particularly on the negative side. Overall, the curated distribution is shifted towards more moderate and positive changes, potentially introducing a small bias. In total, 41% of the points are retained, with the highest fraction in the central Arctic (up to 65%, Figure 2b).

4 Results

The first part of the results quantifies the contributions shaping sea-ice thickness change (Section 4.1), highlighting the importance of dynamical thickening, dynamical thinning, and lead ice growth. This motivates the second part, which examines the long-term trend in dynamic thickness change and deformation (Section 4.2). Section 4.3 addresses the uncertainties and limitations of these results.

https://doi.org/10.5194/egusphere-2026-3122
Preprint. Discussion started: 11 June 2026
© Author(s) 2026. CC BY 4.0 License.

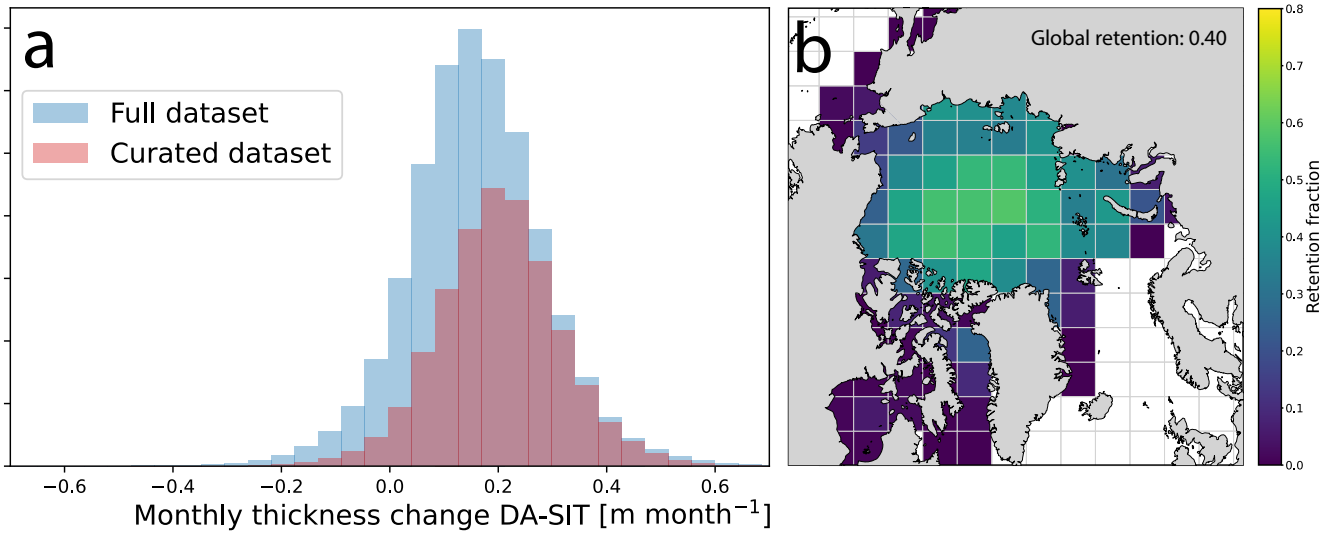


Figure 2. (a) Distribution of DA-SIT monthly thickness change for the full dataset and the curated dataset (pan-Arctic, all years). The two distributions closely overlap (Kolmogorov–Smirnov test, KS = 0.16), indicating that the curation preserves the overall characteristics of the original dataset. (b) Map of the Arctic ocean. Grid cells are colored by their retention fraction after applying the stage 2 agreement filter.

4.1 Thermodynamic and dynamic contributions to pan-Arctic Lagrangian thickness change

Figure 3 compares mean sea-ice thickness and monthly thickness change from DA-SIT and Icepack over the full study period and decomposes the Icepack thickness change into thermodynamics, dynamical thickening, dynamical thinning and lead ice growth. Both DA-SIT and Icepack show the expected regional thickness distribution, with the thickest ice north of Greenland and within the convergence/stagnation zone of the Transpolar Drift, and thinner ice in the marginal seas. This spatial contrast is weaker in Icepack than in DA-SIT. The change fields indicate enhanced thickness change along the Transpolar Drift and at the main export gateways (Fram Strait, Bering Strait, and the Canadian Arctic Archipelago), whereas the Beaufort Gyre exhibits weaker changes. Thermodynamic growth is spatially smooth, with a reduced signal in the Atlantic inflow region of the Barents Sea. Dynamical thinning forms a broad peripheral band of negative contribution in grid cells next to the coast, while dynamical thickening shows a similar large-scale structure but is enhanced in the Transpolar Drift convergence zone and in the Chukchi Sea. Lead ice growth is weaker overall and is concentrated mainly in export and divergence regions. Note that, due to different sensor coverages, not all grid cells are evenly surveyed. Figure 3c indicates observations per grid cell and indicates the survey limits of the sensors.

The simulated pan-Arctic mean thickness change of 0.21 m per month is composed of 0.14 m per month thermodynamic thickening, 0.13 m per month dynamical thickening, −0.11 m per month dynamical thinning, and 0.05 m per month lead ice growth. This decomposition highlights two key results: First, dynamical thickening is of comparable magnitude to thermody-

https://doi.org/10.5194/egusphere-2026-3122
Preprint. Discussion started: 11 June 2026
© Author(s) 2026. CC BY 4.0 License.

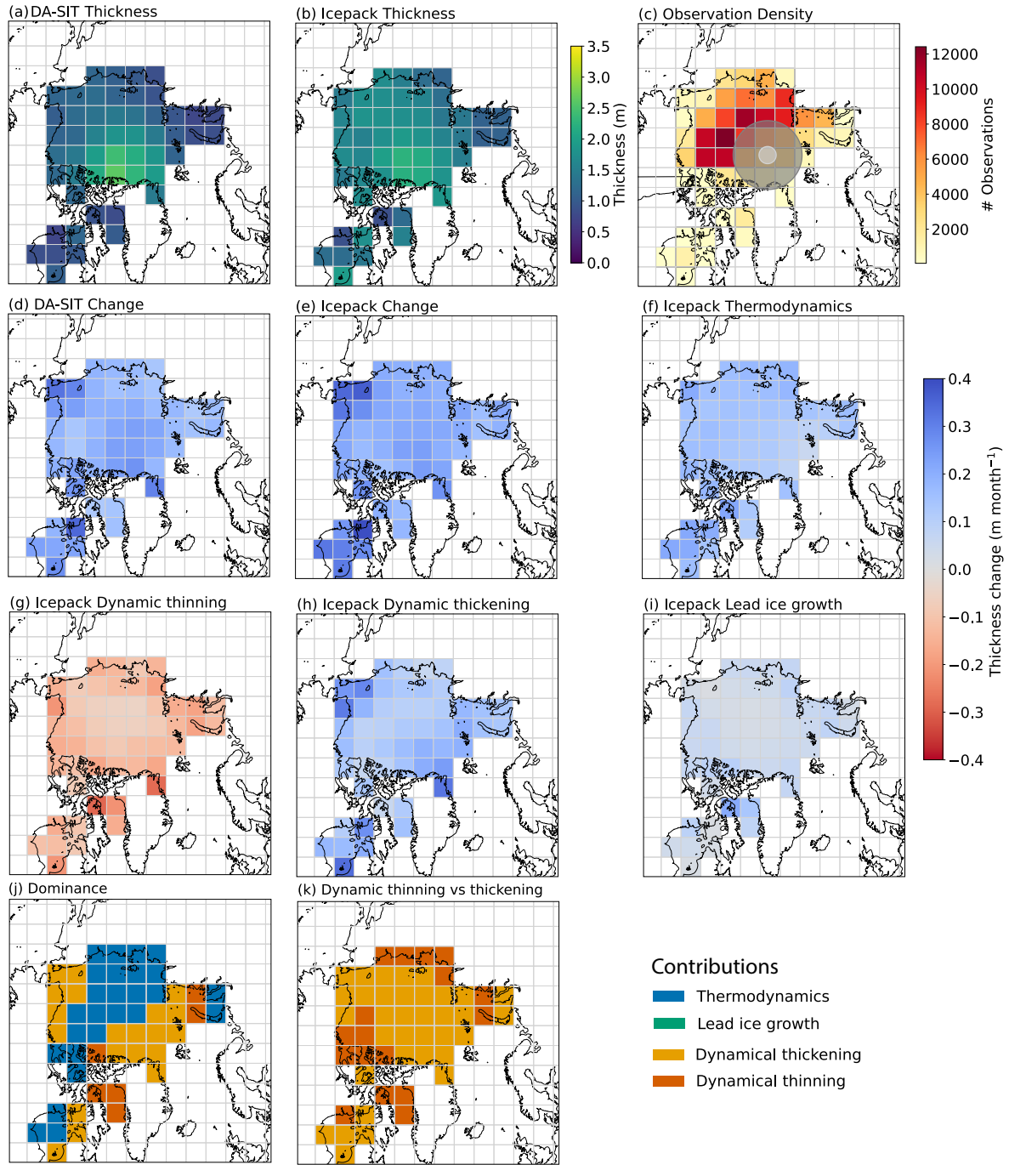


Figure 3. Pan-Arctic mean sea-ice thickness and monthly thickness change for 2002–2020. a: DA-SIT thickness, b: Icepack thickness, c: grid-cell IDs with the number of contributing observations. d: DA-SIT total thickness change, e: Icepack total thickness change, f: Icepack thermodynamics. g: Icepack dynamical thinning, h: Icepack dynamical thickening, i: Icepack lead ice growth, j: Largest contribution to that grid cell. k: Largest contribution but only considering dynamical thickening or thinning. The color legend of the contributions in (j, k) is shown in the lower right corner.

https://doi.org/10.5194/egusphere-2026-3122
Preprint. Discussion started: 11 June 2026
© Author(s) 2026. CC BY 4.0 License.

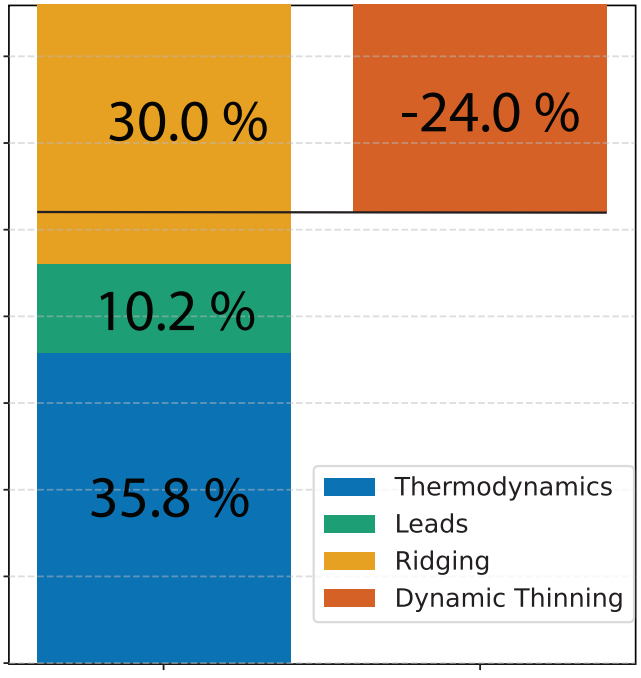


Figure 4. Sea ice thickness budget with the relative contributions of the curated dataset. Since dynamical thinning is negative, it is plotted separately, and the black line marks the signed net change.

namic thickening and is therefore a major contributor to total thickness change. Second, the positive and negative dynamic terms largely offset one another, yielding a much smaller net dynamic contribution of 0.06 m per month.

Figure 4 summarizes the pan-Arctic relative mean contributions calculated from the curated dataset. Relative contributions were calculated along individual trajectories and then averaged to obtain the presented values. To enable a meaningful comparison between the contributions, the numerical values are calculated using absolute magnitudes, i.e. considering thinning as positive, too. Thermodynamics (35.8%) and dynamical thickening (30.0%) are the dominant positive terms, whereas dynamical thinning reduces the ice thickness by -24.0%, partly compensated by 10.2% lead ice growth. The corresponding values for the full (non-curated) dataset are very similar: 35.3% for thermodynamics, 33.5% for dynamical thickening, -22.0% for dynamical thinning, and 9.3% for lead ice growth. This indicates that the second stage curation has only a minor effect on the Arctic-wide partitioning of the thickness contributions. The main difference is a modest redistribution between dynamical thickening and thinning.

Figure 5 and 3(f-k) highlight pronounced regional contrasts in the dominance of the contributions. In the export branch of the Transpolar Drift thermodynamic growth dominates, and in several coastal cells dynamical thinning exceeds dynamical thickening (Figure 3k). In the convergence zone north of Greenland, dynamical thickening is the largest contribution (Figure 3j). In the Beaufort Gyre, thermodynamic growth remains dominant (Figure 3j), while dynamical thickening is generally the

https://doi.org/10.5194/egusphere-2026-3122
Preprint. Discussion started: 11 June 2026
© Author(s) 2026. CC BY 4.0 License.

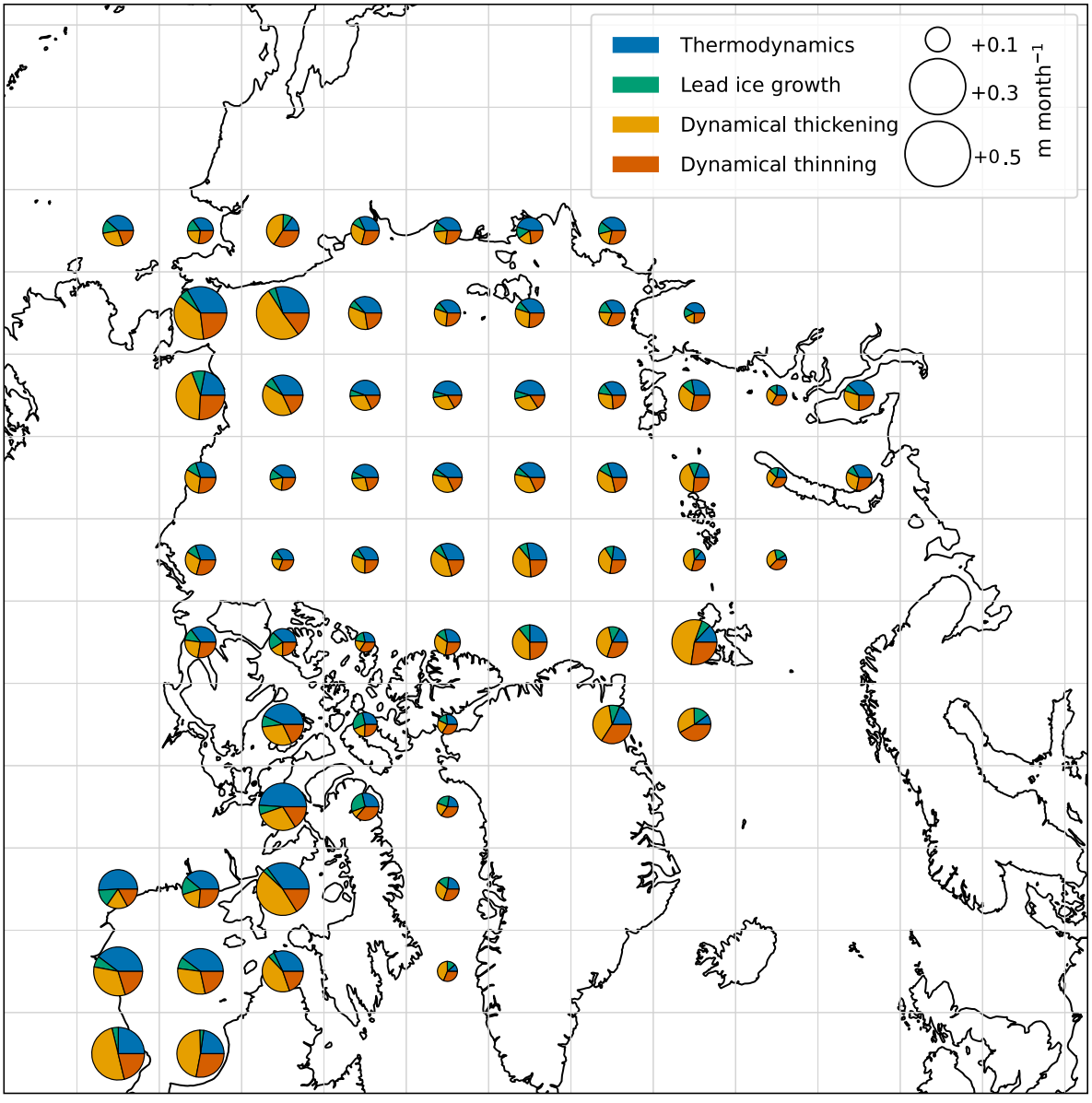


Figure 5. Regional relative contributions to monthly sea-ice thickness change for 2002–2020. Pie charts show the relative magnitude of thermodynamic growth, lead ice growth, dynamical thickening, and dynamical thinning in each grid cell. The size of the pies scales with the magnitude of the absolute total thickness change.

https://doi.org/10.5194/egusphere-2026-3122
Preprint. Discussion started: 11 June 2026
© Author(s) 2026. CC BY 4.0 License.

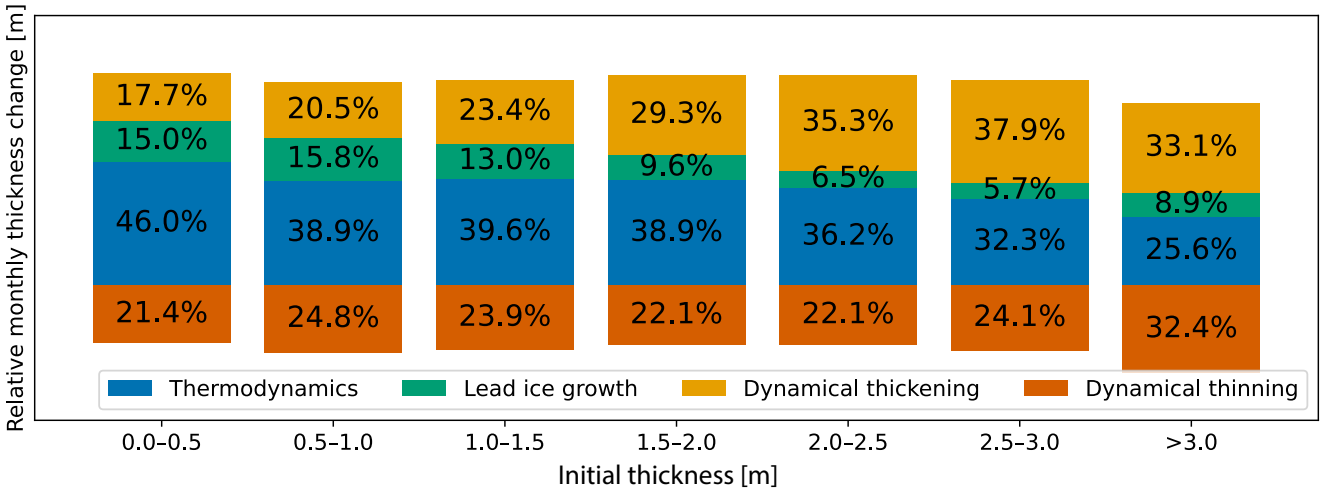


Figure 6. Bar plots of relative contributions to monthly sea-ice thickness change, binned by initial Icepack thickness.

second-largest term, except for the branch close to the Canadian coast. Overall, dynamical thickening exceeds thinning in most central Arctic cells (Figure 3k), whereas thinning is comparatively stronger in export sectors on the Siberian shelf, in Fram Strait and the Canadian Arctic Archipelago. Thermodynamics show a smooth gradient of increasing ice growth from the Atlantic sector, particularly Barents Sea and Kara Sea, towards the Pacific sector. Those regional contrasts are mostly consistent with regional differences in deformation and ocean forcing.

The dependence of the contributions on pre-existing ice thickness supports the physical plausibility of our simulations (Fig. 6). Thermodynamic growth decreases (relative and absolute) with larger initial thickness, as expected from the thin-ice growth feedback, whereas dynamical thickening is larger for thicker ice as the ridged volume increases with larger pre-existing ice thickness and its growing buckling strength (Figure 6, Hopkins, 1998). The lead contribution also decreases with increasing thickness. This could potentially be related to compensating effects of ridged (and thus thicker) ice growing slower than the "pure thermodynamically grown" ice discussed in Section 3.3.3. The thickness dependence of dynamical thinning is negligible, which is in line with the fact that the resistance force of ice against divergence is much weaker than towards compaction and therefore small even for thick ice (Petrich and Eicken, 2017). While there is also a geographically-bound co-dependency between thick ice and dynamical thickening (e.g. Last Ice Area), we observe the characterized dependency independent of the dynamical regime in most grid cells, however, with varying thicknesses at which dynamical thickening outweighs the thermodynamic contribution.

To complement the analysis of monthly relative contributions, Figure 7a shows the seasonal cycle in the absolute positive and negative thickness changes from DA-SIT and Icepack. Both datasets exhibit a clear seasonal cycle in the positive thickness changes while Icepack shows larger changes and reaches a maximum in January, a month earlier than DA-SIT (February). In contrast, negative thickness change shows no distinct seasonal cycle. Interestingly, the fraction of the thickness contributions stays almost constant (not shown) because the absolute contributions of thermodynamics and dynamical thickening increase

https://doi.org/10.5194/egusphere-2026-3122
Preprint. Discussion started: 11 June 2026
© Author(s) 2026. CC BY 4.0 License.

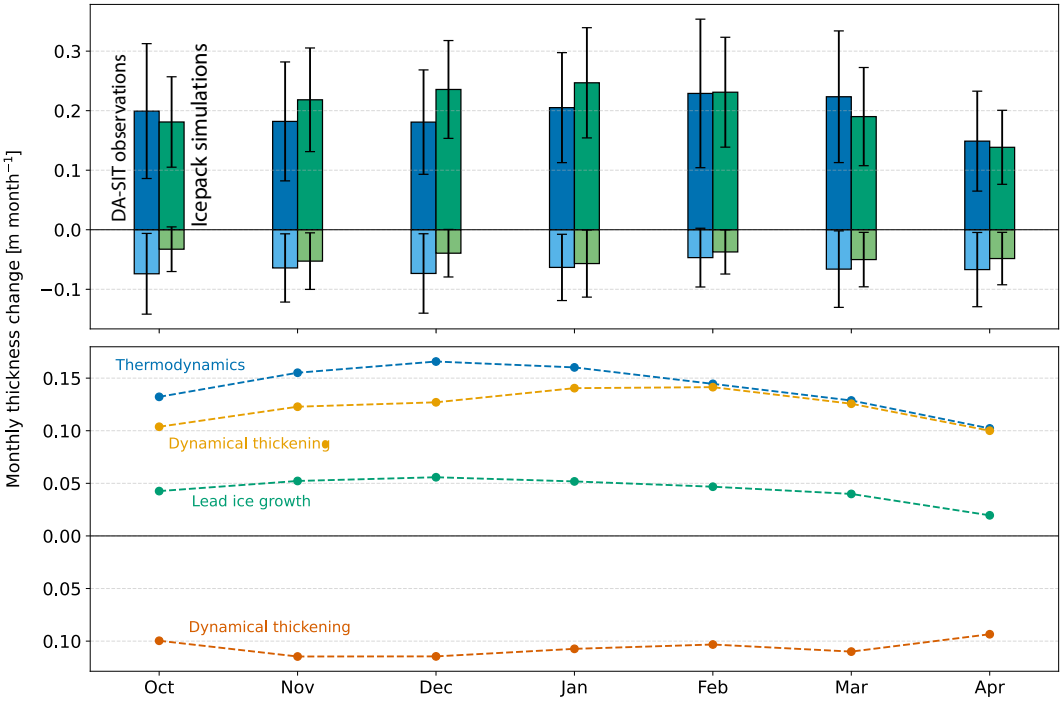


Figure 7. Monthly mean positive and negative sea-ice thickness changes from DA-SIT and Icepack for October–April, averaged over 2002–2020. a: total change with positive and negative changes are shown separately for each month. Bars indicate the monthly means and error bars denote $\pm 1\sigma$. b: absolute contributions to thickness change from Icepack.

and decrease in a very similar manner (Figure 7b). They differ, however, in the timing of the maximum with an earlier peak in the thermodynamics in December and a later peak in dynamical thickening in February. The thermodynamic pattern is most likely explained by a combination of the thermodynamic forcing and the ice-growth feedback that slows down the growth when the ice becomes thicker. The seasonal cycle in dynamical thickening could be explained by a superposition of decreasing deformation rates (Fig. 11b) and increasing ice thickness towards spring.

Last, we examine interannual variability over the 2002–2020 period (Figure 8). To avoid a bias related to the different sensor coverage of Envisat and CryoSat-2, we selected a subset of the central Arctic that is covered by both sensors (see Figure 10c and d for coverage). For this subset, differences between Envisat and CryoSat-2 during the overlap seasons 2010/11 and 2011/12 are small, except for the CryoSat-2 estimate of dynamical thickening in 2010/11, which is larger than the corresponding Envisat estimate (yellow shading in Figure 8). We observe a weak increase in dynamical thickening of 2.2% per season that is most pronounced after 2013/2014 (purple shading) of about 0.04 m per month. The other components show no trend but the thermodynamic component peaks in the seasons 2007/2008 and 2013/2014.

In summary, dynamic thickness change provides a net positive contribution to the Arctic winter sea-ice budget. When separated into dynamical thickening, thinning, and lead ice growth, the absolute dynamic contributions are comparable in

https://doi.org/10.5194/egusphere-2026-3122
Preprint. Discussion started: 11 June 2026
© Author(s) 2026. CC BY 4.0 License.

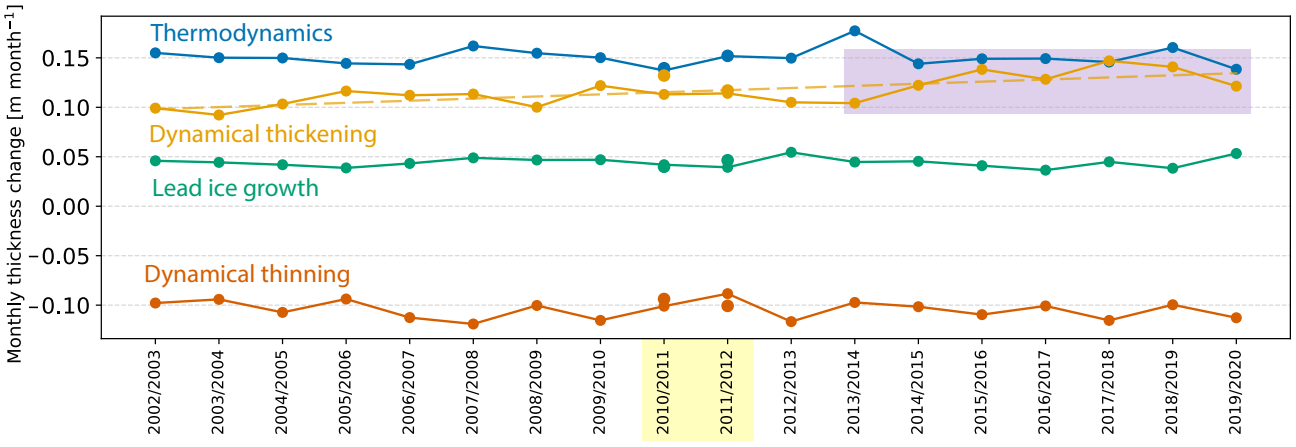


Figure 8. Pan-Arctic contributions to monthly sea-ice thickness change for each winter season from 2002–2020 for the common subset of Envisat and CryoSat-2. The time period of most pronounced changes in the dynamical thickening is marked in purple. The dashed line shows the linear trend with a slope of 2.2%. The overlap seasons 2010/2011 and 2011/2012(03) are highlighted in light yellow and the two estimates from both sensors are plotted.

magnitude to thermodynamic growth. Despite strong regional contrasts, the positive dynamic terms consistently contribute at least about one third of the total thickness change, highlighting their importance even in weakly dynamic regimes. Their pan-Arctic relevance and the observed, small positive trend in dynamical thickening raises a need to better understand the variability and long-term evolution of the dynamic processes, which is addressed in Section 4.2.

4.2 Long-term evolution of dynamic thickness change and deformation

The small positive long-term trend in dynamical thickening (Figure 8) motivated further analysis of a potential wintertime negative dynamic feedback, in which thinner ice experiences enhanced dynamical thickening counteracting further thinning.

We base this analysis primarily on the observations, i.e. thickness from DA-SIT and the deformation derived along the trajectories (Section 3.2). Total deformation, calculated from shear and divergence, is accumulated into monthly aggregates along the trajectories and subsequently gridded according to the trajectory locations. We further analyze the net dynamic sea ice thickness change from DA-SIT, DA-SIT$_{\mathrm{dyn}}$, which is estimated by subtracting the respective Icepack thermodynamic contribution from the total thickness of DA-SIT. This approach provides an estimate of the dynamic component that is independent of deformation forcing, in contrast to the model-derived dynamic thickening and thinning contributions.

We note that DA-SIT$_{\mathrm{dyn}}$ includes residual uncertainties; however, these are expected to be small due to the applied data curation (Section 3.4). To avoid biases arising from differing sensor coverage between Envisat and CryoSat-2, we restrict the long-term analysis (2002–2020) to grid–month pairs consistently observed by both sensors in each season. This results in 90 spatial–temporal samples per year, with most observations occurring between December and March, and fewer in October,

https://doi.org/10.5194/egusphere-2026-3122
Preprint. Discussion started: 11 June 2026
© Author(s) 2026. CC BY 4.0 License.

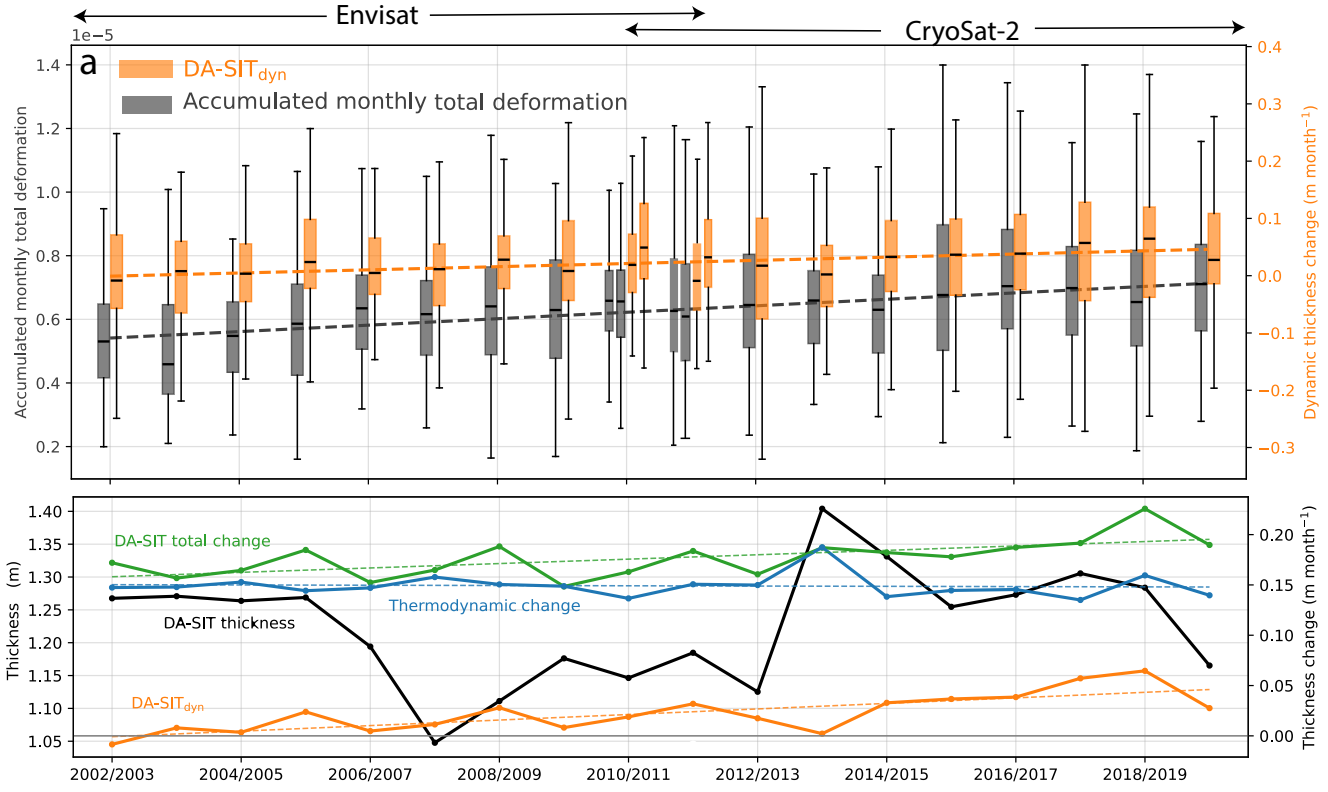


Figure 9. Pan-Arctic boxplot time series of accumulated monthly total deformation, DA-SIT$_{\mathrm{dyn}}$, DA-SIT thickness, DA-SIT thickness change, and Thermodynamics. (a) Boxplots of accumulated monthly total deformation (gray, left y-axis) and DA-SIT$_{\mathrm{dyn}}$ (orange, right y-axis). Boxplots are calculated from the common subset of both altimeters, consisting of 90 month–grid-cell pairs for each season. Dashed lines indicate linear trends in the medians. The overlap period is shown by two bars, with Envisat first and CryoSat-2 second. (b) Time series of medians for DA-SIT thickness (black, left y-axis) and DA-SIT total thickness change (green, right y-axis), Thermodynamic change (blue, right y-axis) and DA-SIT$_{\mathrm{dyn}}$ (orange, right y-axis). Dashed lines show linear trends. 2010/2011 displays Envisat, 2011/2012 displays CryoSat-2 data.

November, and April. We further calculate medians for each grid–month pair before applying further statistics like trend estimates to reduce a regional (or temporal) bias from grids (months) that contain more observations.

Figure 9 shows the pan-Arctic long-term evolution of the analyzed subset, including dynamic and thermodynamic thickness change, total thickness, and accumulated deformation. Known differences in sensor-specific uncertainties in Envisat (before and after 2008) and CryoSat-2 (Khvorostovsky et al., 2020; Bocquet et al., 2024), limit the interpretability of long-term thickness changes (Figure 9b, black). Despite the lack of a significant and safely-interpretable trend, substantial interannual variability in thickness is evident, with fluctuations on the order of 0.2–0.3 m across the record.

https://doi.org/10.5194/egusphere-2026-3122
Preprint. Discussion started: 11 June 2026
© Author(s) 2026. CC BY 4.0 License.

The positive trend in total sea ice thickness change (Figure 9b, green) is primarily driven by DA-SIT$_{\mathrm{dyn}}$ (Figure 9a,b, orange), whereas the thermodynamic contribution remains comparatively stable over time, with only two notable positive anomalies in 2007/2008 and 2013/2014 (Figure 9b, blue). Over the full period (2002–2020), DA-SIT$_{\mathrm{dyn}}$ exhibits a positive, significant ($p < 0.001$) trend of 0.27 cm per month per season (12% relative to the mean), corresponding to 5 cm per month more monthly growth after 18 years. There is significant seasonal and regional variability which is reflected in the spread of the boxplots but difficult to quantify because most individual grid cell and monthly trends are insignificant (see Figure 10d). We further note that for the full (non-curated) dataset there is also a positive trend, however, DA-SIT$_{\mathrm{dyn}}$ is negative (thermodynamics > DA-SIT change), approaching zero towards 2020. For our spatial and temporal subset, we also observe a small, significant ($p< 0.001$) positive trend in the accumulated monthly total sea ice deformation (Figure 9b, gray). The trend magnitude is small with an increase of $1 \times 10^{-7}\mathrm{s}^{-1}$ per season or 1.6% per season relative to the mean. The spread of the boxplots reflects the regional and seasonal variability.

Interpreting regional trends in deformation and dynamic thickness change is challenging because the long-term analysis is limited to a subset of the Arctic. To complement this, we additionally analyze the CryoSat-2 period (2010/2011–2019/2020) exclusively to provide broader spatial coverage while acknowledging that the trends are not significant due to their short duration.

Figure 10 illustrates the spatial variability of interannual trends at individual grid cells. Over the full time series, positive deformation trends dominate most grid cells (Figure 10c). In contrast, during the shorter CryoSat-2 period, the pan-Arctic deformation trend becomes negligible in the central Arctic, with regionally contrasting patterns: positive trends in the Beaufort Gyre and neutral to negative trends in the Transpolar Drift.

A similar shift is evident for DA-SIT$_{\mathrm{dyn}}$ (Figure 10b,d). The overall positive trend observed over the 2002–2020 period (d) weakens considerably during the CryoSat-2 era (b), with several regions transitioning toward neutral or negative trends. The Transpolar Drift and in particular the convergence zone north of Greenland not covered in the long-term evolution exhibit negative trends in dynamic thickness change.

Overall, the analysis reveals a consistent but weak positive trend in deformation alongside an increase in dynamic thickness change over the full 2002–2020 period. While thermodynamic contributions remain largely stable, dynamic processes dominate the long-term evolution of the interannual thickness change. Positive thickness change and deformation trends seem to be stronger in time periods that experienced stronger thickness changes (early winter vs late winter Bocquet et al., 2024), and weaken when restricting the analysis to the more recent 2010–2020 years.

4.3 Uncertainties and limitations of the observed and modeled Lagrangian sea ice thickness change

Both observed and simulated sea-ice thickness changes are subject to different sources of uncertainty. The following subsections quantify the uncertainties of the altimeter-derived thickness observations (Section 4.3.1) and the Icepack simulations (Section 4.3.2), and discuss the model-observation misfit as an approximation of the total uncertainty (Section 4.3.3). Unless stated otherwise, we use the median to represent the systematic component of the uncertainty and the MAD for the random component.

https://doi.org/10.5194/egusphere-2026-3122
Preprint. Discussion started: 11 June 2026
© Author(s) 2026. CC BY 4.0 License.

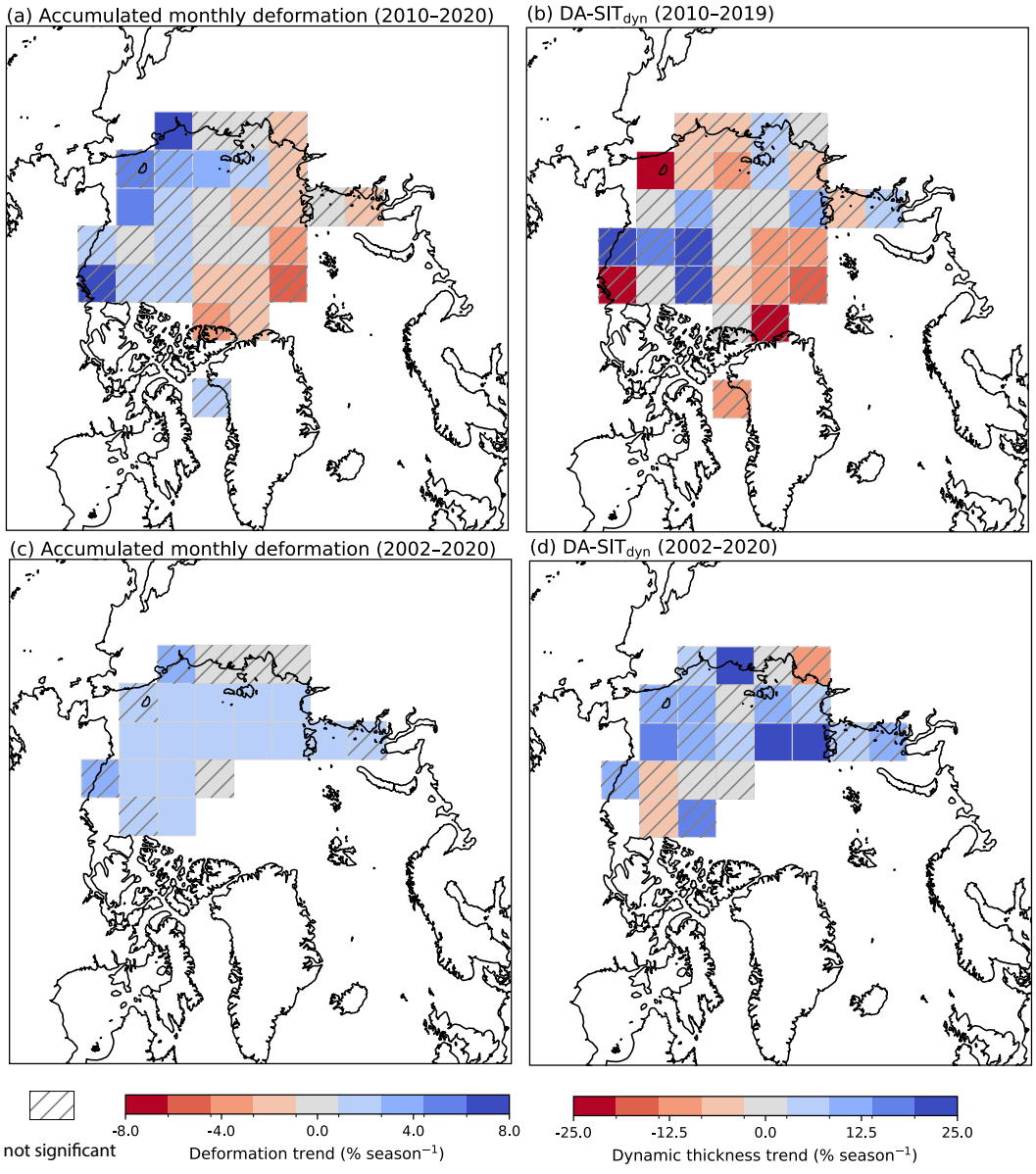


Figure 10. Spatial distribution of interannual trends in accumulated monthly deformation and dynamic thickness change (DA-SIT$_{\mathrm{dyn}}$) at the grid-cell level. Panels (a–b) show trends for the CryoSat-2 period (2010/2011–2019/2020), while panels (c–d) show trends for the full period (2002–2020) restricted to the common grid–month subset. Colors indicate the magnitude and sign of the linear trend, with red (blue) representing negative (positive) trends. Hashed grid cell trends are not significant.

https://doi.org/10.5194/egusphere-2026-3122
Preprint. Discussion started: 11 June 2026
© Author(s) 2026. CC BY 4.0 License.

4.3.1 Uncertainty of the altimeter-derived thickness observations

Spatial and temporal representation uncertainty

When averaging trajectories that sample different ice within our circle of interest, a spatial and temporal representation uncertainty is introduced. The sampled ice may not be fully representative of the entire area and systematic variations, for example due to the systematic change in satellite orbits, can introduce oscillatory variability in the obtained mean thickness. As this representation uncertainty strongly depends on spatial and temporal scales, we performed a simplified scaling analysis to identify the scales that minimize this uncertainty. We evaluated the representation uncertainty across different circle radii (50–500 km) by comparing independent mean sea-ice thickness measurements during periods of minimal deformation (<1% per day; see Appendix 7.2). Based on this analysis, we selected a radius of 250 km and a 30-day running mean, as these minimize representation uncertainty while still distinguishing different ice regimes and capturing the temporal thickness changes expected at these scales. The remaining median difference of 0.16 m between independent observations aligns well with the expected average thermodynamic contribution (0.14 m per month), suggesting a small systematic uncertainty (0.02 m per month). The negligible unexplained difference further supports the assumption that measurement uncertainties (see above) strongly co-vary on monthly timescales. The MAD of 0.11 m may indicate the random component of the representation uncertainty; however, this value also includes thickness retrieval uncertainties and variability in thermodynamic growth.

DA-SIT thickness retrieval uncertainty

For each parcel along a trajectory (cell average over the 75 km spatial resolution of DA-SIT), DA-SIT provides the mean thickness retrieval uncertainty, originally derived from the Level-2 along-track SIT of the CCI climate data record (version 3.0), assuming that all measurements within a parcel are uncorrelated (Ricker et al., 2025a). Since the uncertainty budget is dominated by geophysical properties varying rather slowly in time (e.g., snow depth, ice and snow densities, e.g., Willatt et al., 2011; Nandan et al., 2017; Khvorostovsky et al., 2020), we further assume these uncertainties to be strongly correlated over the 30-day averaging window. The validity of this assumption is supported by the scaling analysis (previous subsection) and has two implications for our study. First, applying a 30-day running mean does not substantially reduce the retrieval uncertainty. Thus, when calculating the uncertainty of the 30-day running mean thickness, we conservatively assume an effective sample size of one for the error propagation and calculate the running average of the sample uncertainties. Averaging all DA-SIT retrieval uncertainties (pan-Arctic, all years), the median yields 0.079 m (MAD: 0.015 m). Second, when calculating the uncertainty of the monthly differences, the covariance can be assumed to be large, too. This reduces the uncertainty ($\sigma_{\Delta H}$) of the monthly differences, which can be calculated from the individual uncertainties of the 30-day mean thickness estimates ($\sigma_{\mathrm{start}}, \sigma_{\mathrm{end}}$) by

$$\sigma_{\Delta H}^2 = \sigma_{\mathrm{start}}^2 + \sigma_{\mathrm{end}}^2 - 2\rho\sigma_{\mathrm{start}}\sigma_{\mathrm{end}}, \tag{3}$$

Here, ρ is the correlation between the retrieval uncertainties of the two monthly windows, i.e. $\rho = 0$ corresponds to the two thickness observations being independent, while $\rho = 1$ corresponds to fully correlated ones. As we assume the correlation to

https://doi.org/10.5194/egusphere-2026-3122
Preprint. Discussion started: 11 June 2026
© Author(s) 2026. CC BY 4.0 License.

be between these extremes, we choose $\rho = 0.5$. Averaged (pan-Arctic, all years) this approach yields a median of 0.078 m per month (MAD: 0.014 m per month) for the monthly thickness changes. We note that those uncertainties highly depend on the made assumptions on the unknown covariances and their temporal and spatial variability of the measurement retrieval uncertainties.

Sea ice drift uncertainty

Increasing the lag time of DA-SIT to 7 months increases the uncertainty of the sea-ice drift, which is based on the original sea-ice drift product (OSI SAF, 2022a) and provided with DA-SIT. Calculating the median drift uncertainty across all trajectories yields 18 km. Given the large spatial scale of $500\,\mathrm{km} \times 500\,\mathrm{km}$, this uncertainty slightly blurs the spatial resolution but is negligible for our study design.

4.3.2 Uncertainties of the Icepack simulations

Uncertainty of simulated thermodynamic thickness change

To validate the thermodynamic thickness change in our simulations, we compared simulated thermodynamic thickness change with independent ice thickness observations from 38 IMBs (5146 observations of monthly thickness change; see Section 2.3). ERA5 and CFS-R/v2 were used as atmospheric forcing. Icepack overestimates snow thickness, with smaller biases in CFS-R/v2-forced simulations than in ERA5-forced simulations, while both forcings show similar spread. Despite this, the simulations also overestimate sea ice thickness. ERA5-forced simulations exhibit relatively small biases that correspond well to the mean uncertainty of 0.05 m of the IMBs observations, whereas CFS-R/v2-forced simulations show a stronger overestimation in both absolute thickness and monthly changes. For the ice thickness, ERA5-forced simulations have a median bias of -0.050 m and MAD of 0.081 m (CFS-R/v2-forced simulations: -0.188 m, MAD: 0.102 m). For the monthly changes, the median bias of ERA5-forced simulations becomes smaller and even slightly positive (underestimation of thickness change) with 0.011 m per month and a MAD of 0.041 m per month (CFS-R/v2-forced simulations: -0.036 m per month, MAD: 0.044 m per month). We could further exclude a thickness-dependent and region-dependent bias of the simulations. We concluded that the thermodynamic simulations are highly accurate under predominant growth conditions. Details of the comparison are presented in the Appendix 7.1.

Uncertainty of the dynamic ice thickness change

In contrast to thermodynamic thickness change, validating dynamic thickness change directly against thickness observations is more challenging due to the lack of suitable independent data. We therefore separate the uncertainty into three types, each addressed by using different approaches: (1) uncertainty associated with differing spatial coverage of thickness observations and deformation polygons, as well as random uncertainty in trajectory locations; (2) uncertainty related to the coarse spatial resolution relative to the highly localized nature of sea-ice deformation; and (3) uncertainty related to the choice of ridging parameterization in Icepack.

(1) The first uncertainty combines artifacts of the study design with the random uncertainty of the sea-ice drift product. Because the spatial coverage of thickness observations and deformation polygons may differ slightly, deformation and thickness

https://doi.org/10.5194/egusphere-2026-3122
Preprint. Discussion started: 11 June 2026
© Author(s) 2026. CC BY 4.0 License.

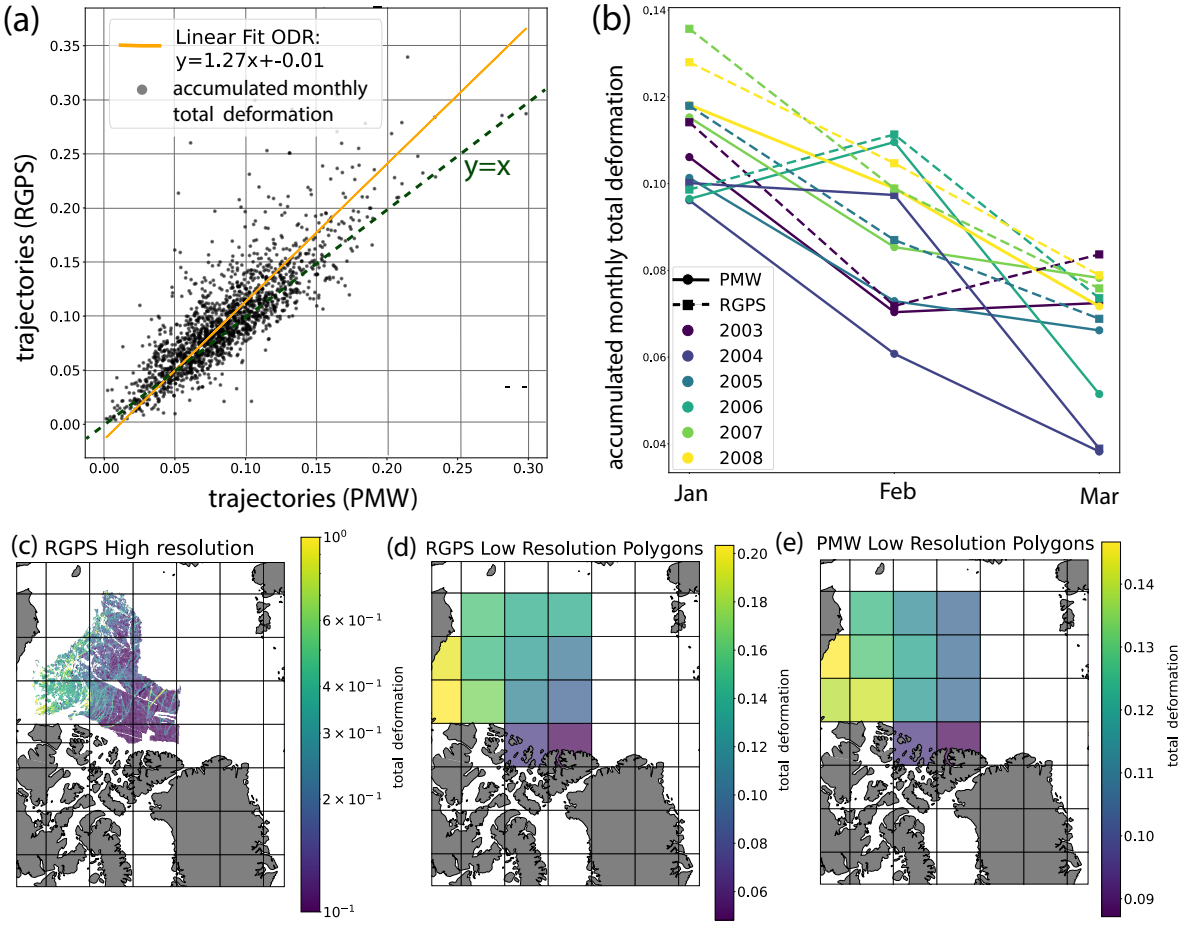


Figure 11. Comparison of accumulated monthly total sea ice deformation derived from the PMW trajectories and the higher-resolution RGPS dataset. (a) Scatter plot of deformation estimates and Orthogonal Distances Regression (ODR) fit. (b) Seasonal cycle (January–March) from RGPS (squares, dashed) and PMW trajectories (circles, solid). (c–e) Spatial representation of deformation across scales for an example month: (c) RGPS data at native resolution (10 km, 3 days); (d) polygon-derived deformation from RGPS drift (10 km, 3 days) regridded to $500\,\mathrm{km} \times 500\,\mathrm{km}$; (e) polygon-derived deformation from PMW drift (75 km, 3 days) regridded to $500\,\mathrm{km} \times 500\,\mathrm{km}$.

change do not always align one-to-one. To estimate the magnitude of this component, we have performed ensemble simulations with 1000 realizations of the deformation forcing for a subset of 50 trajectories. The ensemble spread is designed to represent the variability observed in the deformation estimates derived directly from the observations (see Section 7.3). We noticed that for the individual trajectories, the ensemble spread was small compared to the observation-model misfit. The median of the standard deviations of all ensemble members was 0.027 m (MAD: 0.007) for the total thickness and 0.022 m per month (MAD: 0.006 m per month) for the monthly changes.

https://doi.org/10.5194/egusphere-2026-3122
Preprint. Discussion started: 11 June 2026
© Author(s) 2026. CC BY 4.0 License.

(2) The second uncertainty concerns uncertainties in the sea-ice drift and its coarse spatial resolution relative to the highly localized nature of sea-ice deformation. We evaluate this uncertainty in the deformation forcing by comparison with the higher-resolution RGPS dataset. To do so, we construct time series of polygons (500 × 500 km) with identical starting points based on the PMW-derived DA-SIT trajectories and the nearest RGPS trajectories. We then calculate the total deformation ($\sqrt{\text{divergence}^2 + \text{shear}^2}$) from these polygons, thereby accounting for both divergence and shear, which contribute with similar magnitude to the Icepack forcing. To match the timescale of monthly thickness changes, total deformation is accumulated over one month and subsequently compared between the PMW-based product and the higher-resolution RGPS dataset. Further details of the method are provided in Appendix 7.4.

Overall, the accumulated monthly total deformation shows a strong correlation between both datasets ($R = 0.84$), indicating that the PMW product captures the large-scale variability in deformation magnitude, although with a slight underestimation (ODR slope > 1, Fig. 11a). The seasonal cycle is also well reproduced: both datasets consistently show a decrease in deformation from January to March, and inter-month differences exceed inter-dataset differences, highlighting that the PMW data resolve the dominant seasonal signal present in this regional subset (Fig. 11b). At the regional scale, spatial patterns of deformation are generally preserved, with correlations within individual grid cells (size 500x500 km) ranging from 0.57 to 0.94, demonstrating that the PMW product resolves large-scale gradients across the Arctic basin (not shown). However, case studies reveal that agreement depends on the strength of the deformation signal: strong, well-organized patterns (e.g., January 2008, Fig. 11c-e) are consistently captured, whereas weak or noisy conditions lead to discrepancies between datasets. Figure 11c–e also illustrates how sea-ice deformation appears on 500 × 500 km scales. At high resolution (panel c, RGPS), deformation is concentrated along narrow linear kinematic features, reflecting its localized and intermittent nature. Upon aggregation (panels d–e), these features are no longer resolved and merge into a spatially smooth field. Thus, deformation at this scale should be interpreted not as individual events, but as a spatially averaged regime of deformation. Nevertheless, large-scale gradients, such as enhanced deformation toward the Alaskan coast and reduced deformation toward the central Arctic, remain clearly visible. Interannual variability is partly resolved, as differences between years are generally larger than differences between PMW and RGPS for strong signals, although the signal-to-noise ratio remains limited and smaller year-to-year differences cannot always be robustly detected (see Appendix Fig. 19).

To quantify the uncertainty inherent to the PMW dataset, we computed the median and MAD between PMW and RGPS deformation on the same spatial scale. This yields a median of $-0.005\ \text{s}^{-1}$ with a MAD of $0.013\ \text{s}^{-1}$, corresponding to a relative uncertainty of -5% (MAD: 14%) compared to the mean accumulated monthly deformation of $0.0949\ \text{s}^{-1}$. Both median and MAD show a clear dependence on deformation magnitude, indicating that PMW underrepresents strong deformation events. For small accumulated deformation ($< 0.05\ \text{s}^{-1}$), i.e. quiet phases, the median is even slightly positive (overestimation, $0.0052\ \text{s}^{-1}$). With increasing deformation, the median becomes increasingly negative, following a linear relationship (slope ~ -0.3) until it breaks down beyond $\sim 0.2\ \text{s}^{-1}$ due to limited data (median: $-0.034\ \text{s}^{-1}$). The MAD increases simultaneously from 0.0056 to $0.0230\ \text{s}^{-1}$, before becoming unreliable at higher deformation rates. To translate those numbers into thickness change, we used a simple first-order scaling of $\alpha = 1$–3 between deformation and dynamic thickness change ($\Delta h_{\text{dyn}} = \alpha\ \epsilon_{\text{monthly,acc}}$) which is derived from the observed range of accumulated deformation and thickness change

https://doi.org/10.5194/egusphere-2026-3122
Preprint. Discussion started: 11 June 2026
© Author(s) 2026. CC BY 4.0 License.

and which corresponds well to the typical ice thickness. Thus, the systematic uncertainty of the deformation forcing corresponds to 0.005–0.015 m per month (MAD: $0.013 - 0.039$ m per month) with a "noise floor" for quiet dynamic regimes of $0.0052 - 0.0156$ m per month.

We conclude that PMW-derived deformation captures regional, seasonal and – within limits – interannual variability at 500×500 km and monthly scales, but systematically smooths deformation magnitudes and underrepresents localized intermittent events (Fig. 11c–f). A non-negligible noise floor is present during quiet phases. These results are specific to this dataset and should not be generalized.

(3) To thoroughly characterize the uncertainty related to the choice of the ridging parameterization in Icepack, higher-resolution observations would be required, as Icepack was originally developed for climate-model resolutions of typically $25\,\mathrm{km} \times 25\,\mathrm{km}$ grid cells and hourly to daily timescales. Nevertheless, we make two relevant observations. First, at our scales, the dynamic regime "uniform ice" shows greater skill in resolving dynamic thickness change than "open water", which is particularly evident for larger dynamic thickness changes. Second, we find that the use of the "uniform ice" configuration in Icepack can, in some cases, lead to unrealistic thickening in strongly convergent regimes, as already thick ice is further ridged into unrealistically thick ice. This highlights that, in some cases, a column model such as the applied Lagrangian Icepack, lacking a feedback between deformation forcing and thickness, can produce unrealistic results and requires careful consideration. In this study, such unrealistic trajectories were removed during the initial quality control procedure (Section 3.4).

4.3.3 Total uncertainty and structural limitations from model-observation misfit

So far, we have quantified the uncertainties of the DA-SIT observations and Icepack simulations independently. As uncertainties from observations and model simulations may either compound or cancel each other, the total uncertainty represents a non-trivial combination of both. Although the model–observational misfit cannot strictly be interpreted as the total uncertainty, it can nevertheless provide valuable insights into how different components of the uncertainty budget combine and help identify systematic limitations. We therefore examine the model-observation misfit as a proxy for the total uncertainty and its dependency on the dynamic regime in the following.

The curated 30-day running mean sea ice thickness time series from DA-SIT and Icepack agree within a median bias of -0.267 m (DA-SIT–Icepack, MAD: 0.235 m). Icepack reproduces the observed monthly change with only a small median difference of -0.016 m per month (MAD: 0.061 m per month). In relative terms, this shows that the systematic differences between the simulations and observations are small (8% of the mean monthly thickness change), while their random component is large (MAD corresponding to 29% of the mean monthly thickness change).

Analyzed in more detail, the distribution of the observation-model residuals reveals that while most residuals are within $\pm$ 0.1 m per month, the distribution is skewed towards negative values, indicating that small thickness increases tend to be overestimated. We further explored the model-observation misfit in a density and box plot (Figure 12). The density plot (Fig. 12a) for total thickness change shows strong directional agreement between DA-SIT and Icepack (cosine similarity, $\cos(\theta) =$

https://doi.org/10.5194/egusphere-2026-3122
Preprint. Discussion started: 11 June 2026
© Author(s) 2026. CC BY 4.0 License.

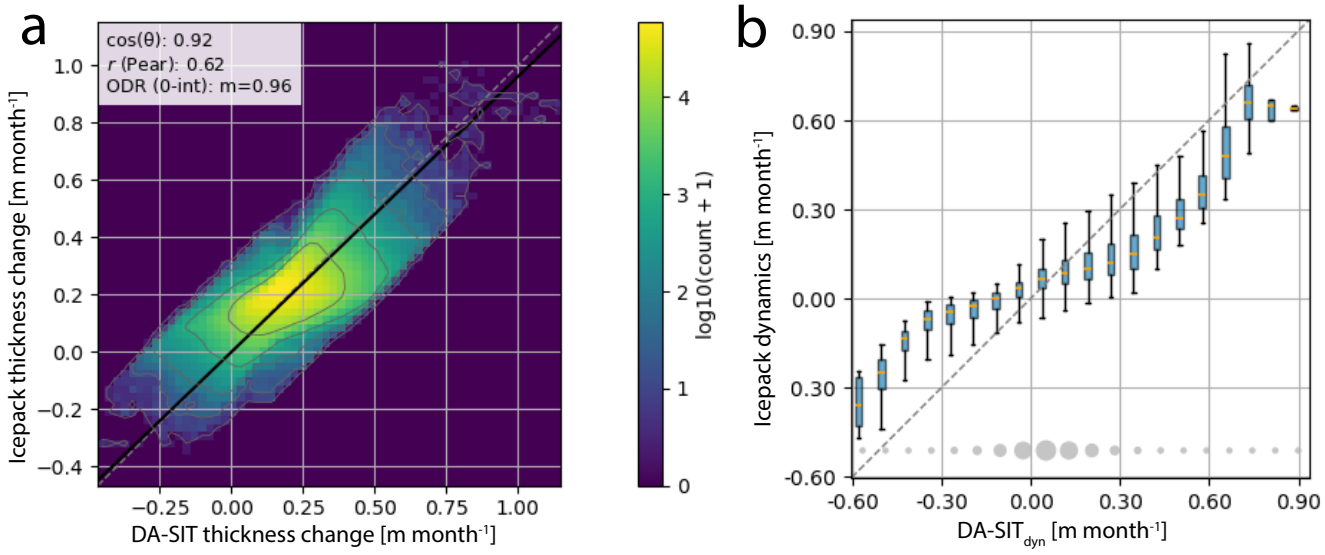


Figure 12. Model–observation misfit between DA-SIT and Icepack monthly thickness change. (a) Density scatter plot of total thickness change. Bright colors indicate a high number of observations. Cosine similarity, Pearson correlation coefficient and ODR (with zero intercept) at the top left express similarity. (b) Binned comparison (boxplots) of Icepack dynamic thickness change versus DA-SIT$_{\mathrm{dyn}}$. Orange lines represent the median of a thickness class. The dashed line indicates the 1:1 relationship. Gray dots at the bottom scale with the number of points within each bin (see also a).

0.92) and an almost unbiased amplitude fit (ODR slope $m = 0.96$). Most changes cluster around 0.1–0.3 m per month which fits well the magnitude of the thermodynamic component. For an in-depth analysis of the dynamic component, we subtracted the thermodynamic component of the Icepack simulations from both the simulated and DA-SIT thickness changes. This yields a scatter plot of (Icepack dynamics $\pm$ uncertainties) versus (DA-SIT total - Icepack thermodynamics $\pm$ uncertainties). When the thermodynamic component is removed, the points cluster indeed around zero ($\overline{\Delta h} \sim 0$) and the agreement weakens markedly, with $\cos(\theta)$ dropping from 0.92 to 0.73 and the ODR slope from 0.96 to 0.68. This shows that the apparent overall model skill is dominated by common thermodynamic-growth conditions. Second, the smaller ODR fit indicates that the dynamic amplitude is systematically damped for larger dynamic changes. This becomes even clearer when binning the changes (Figure 12b). The figure allows us to explicitly assess the ability of the simulations to simulate small and large thickness changes without being biased by the much more frequent small changes. Figure 12b reveals a compressed dynamic response: Icepack overestimates small dynamic thickness changes around zero, but underestimates both strong negative and strong positive events beyond about $|0.25|$ m per month. In other words, the model evens out the extremes and pulls the dynamic signal towards moderate values. We further explore potential mechanisms for this attenuation of the thickness changes. Splitting the monthly changes into different bins according to initial ice thickness reveals contrasting behaviour in DA-SIT and the simulations (Fig. 13): the simulations overestimate thickness change up to an initial thickness of 1.5 m, while they slightly underestimate thickness

https://doi.org/10.5194/egusphere-2026-3122
Preprint. Discussion started: 11 June 2026
© Author(s) 2026. CC BY 4.0 License.

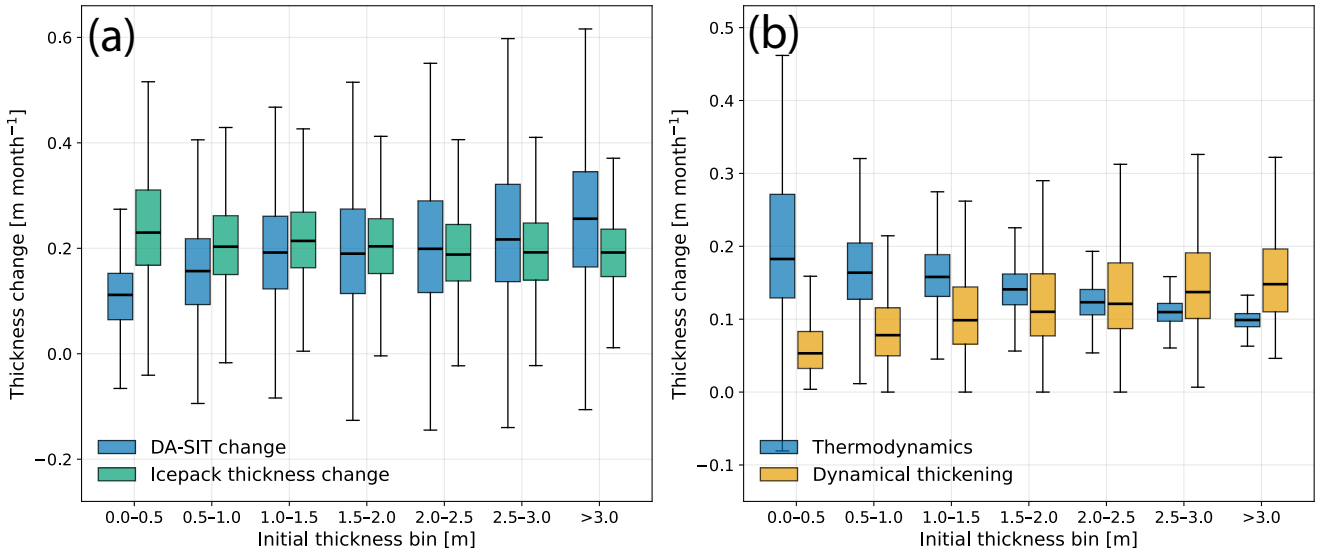


Figure 13. Dependence of monthly thickness change on initial ice thickness for DA-SIT observations and Icepack simulations. Boxplots show binned thickness changes for different initial thickness classes. (a) DA-SIT and Icepack total change binned to the initial thicknesses. (b) Icepack thermodynamics and dynamical thickening binned to the initial thickness.

change in thicker ice. This discrepancy is consistent with (a) an overly strong thermodynamic growth feedback for thin ice in Icepack overestimating thermodynamic thickness change for thin ice and underestimating it for thick ice and; (b) a ridging response that is too weak in Icepack due to too smooth deformation forcing or model physics, as dynamical thickening shows a positive relationship between initial ice thickness and thickness change.

Taken together, across regimes, the most common cases are ice thickness changes of 0.1–0.3 m, which correspond to dynamically quiet conditions and have the smallest observation-model misfit; these are the cases Icepack tends to overestimate the thickness change. By contrast, dynamically active cases, which appear less often, with monthly changes >0.25 m per month are generally underestimated with observation-model misfit increasing roughly linearly up to about 0.5 m per month. This pattern is consistent with uncertainty (2) identified in the deformation forcing (Section 4.3.2, *Uncertainty of the dynamic ice thickness change*), which underestimates large deformation rates by about 30%, exhibits a constant noise level in quiet regimes, and shows increasing uncertainty with deformation magnitude in more active regimes. Thus, the most likely cause of the largest part of the observation-model misfit is that the PMW deformation forcing is too smooth in space and time: weak events occur too frequently, while strong events are too rare or too weak. In addition, a substantial noise floor in the sea ice deformation forcing introduces spurious dynamic thickness changes during quiet periods where none should occur.

https://doi.org/10.5194/egusphere-2026-3122
Preprint. Discussion started: 11 June 2026
© Author(s) 2026. CC BY 4.0 License.

5 Discussion

5.1 The sea ice thickness budget

Our key result is that a small Arctic-mean net dynamic term (0.02 m per month, excluding the thermodynamic lead ice growth here for better comparability) does not imply weak dynamics. Instead, positive contributions from dynamical thickening are largely offset by dynamical thinning. The unique Lagrangian framework of this study allows us to separate opposing dynamic contributions and explicitly quantify their role in the thickness budget. In contrast to most previous studies that consider only net dynamic effects, we show that dynamic thickness change is substantial, contributing at least about one third to total thickness change when considered separately, even in dynamically quiet regimes.

Direct comparison of the dynamic contribution with previous work requires caution due to two key methodological differences. First, most basin-scale studies adopt an Eulerian perspective that includes advection across fixed regional boundaries, whereas our Lagrangian approach neglects ice export through Arctic gateways considering only trajectories of ice present on April 30 of each season. Consequently, we do not provide a closed Arctic-wide mass budget, but instead quantify the processes governing thickness change along the drifting ice. Second, we explicitly separate dynamical thickening, dynamical thinning, and lead ice growth, while most previous studies aggregate these processes into a single dynamic and a thermodynamic term. Those methodological differences explain why previous pan-Arctic studies often concluded that thermodynamic processes dominate over a small (negative) dynamic contribution (Stroeve et al., 2018; Ricker et al., 2021; Anheuser et al., 2023; Koo et al., 2021; von Albedyll et al., 2021; Heorton et al., 2025), and found evidence for strong net dynamic contributions of up to 50% only for (sub-)regional scale dynamic (extreme) events (Kwok and Cunningham, 2016; Itkin et al., 2018; von Albedyll et al., 2021).

In contrast to absolute contributions, regional patterns are more easily compared and show good qualitative agreement across studies. The dominance of thinning over dynamical thickening along the Siberian coastline (except for the Chukchi and East Siberian seas), as well as in parts of the Beaufort Gyre, Nares Strait, and Baffin Bay (Fig. 3k), closely corresponds to regions of negative residuals attributed to thinning in Anheuser et al. (2023, , their Figure 3). In addition, we provide further evidence, consistent with Ricker et al. (2021) and Anheuser et al. (2023), for substantial positive dynamic thickness change in the Chukchi Sea. This also agrees with the observation of larger sea-ice roughness from laser altimetry in this region (Duncan and Farrell, 2022) and highlights the potential influence of land boundaries on Arctic deformation patterns. Because we track moving ice parcels over time in our Lagrangian framework, this study distinguishes between places where deformation has actually occurred and places where already-deformed ice is transported to. In this way, our results complement studies that characterize deformation-prone regions based on ice properties like surface roughness (e.g., Duncan and Farrell, 2022).

New ice growth in leads, i.e., the additional ice that would not have formed without divergence opening the leads, was not explicitly resolved in previous budget studies. Our estimate of 0.05 m per month (24% of the net thickness change) confirms their role as efficient winter ice-production sites and is at the upper end of previous estimates of 0.03–0.05 m per month (Pacific sector, 1997–2000 Kwok, 2006) and 0.02 m per month (Transpolar Drift, 2019/2020 von Albedyll et al., 2022).

https://doi.org/10.5194/egusphere-2026-3122
Preprint. Discussion started: 11 June 2026
© Author(s) 2026. CC BY 4.0 License.

The thermodynamic contribution is easier to compare with, and is essentially consistent with, previous observational estimates. The pan-Arctic mean thermodynamic growth of 0.14 m per month (plus 0.05 m per month from lead ice growth, often included in the thermodynamic component) agrees well with reported winter growth rates (Transpolar Drift: 0.16 m per month (von Albedyll et al., 2022), Transpolar Drift: 0.18 m per month(Koo et al., 2021), pan-Arctic: 0.1–0.4 m per month (Anheuser et al., 2023; Ricker et al., 2021)). While thermodynamic growth was found to be relatively homogeneous across the Arctic, reduced growth in the Barents Sea likely reflects enhanced oceanic heat flux and rising air temperatures (Ricker et al., 2021).

This study provides valuable insights into the sea ice thickness budget, improving our understanding of the current Arctic sea ice system and its potential future evolution in several ways. First, the quantified budget terms, together with their uncertainties, provide a valuable framework for interpreting biases in sea ice thickness in climate and sea ice models. Resolving individual mass-budget components enables model-observation differences to be attributed to specific physical processes rather than bulk quantities, thereby facilitating more targeted model development (Keen et al., 2021; Anheuser et al., 2024). Second, the substantial dynamic contribution also implies a strong dynamic control on ice topography, emphasizing the importance of deformed ice. This has direct consequences for key processes coupling sea ice to other compartments, including air–ice and ocean–ice drag formulations (e.g., Mchedlishvili et al., 2023), and consequently, sea ice drift speeds, ocean–atmosphere heat and gas exchange in leads, melt pond coverage (e.g., Fuchs et al., 2025; Buth et al., 2025), snow source and sink (e.g., Clemens-Sewall et al., 2023; Itkin and Liston, 2025), and ecosystem habitats (e.g., Castellani et al., 2025; Olsen et al., 2026; Müller et al., 2026, and references therein). Finally, thermodynamic and dynamic processes are expected to respond differently to a changing climate. The following section discusses their respective feedback and implications for the future evolution of Arctic sea ice.

5.2 The negative winter dynamic thickness feedback

We explore the hypothesis, previously formulated by Krumpen et al. (2025) for ridge morphology, that thinner ice, associated with an increased first-year ice fraction, leads to more deformation in the Arctic, which, in turn, creates more ridges that increase sea ice thickness.

This negative winter dynamic thickness feedback comprises two components: First, thinner and more dynamic ice cover is more susceptible to deformation (Fig. 14, light green, Rampal et al., 2009) because the force required to build a ridge scales with the buckling strength of ice that is proportional to the initial ice thickness (Hopkins, 1998). Thinner ice therefore reaches this threshold more often under unchanged forcing. While the magnitude of this effect depends strongly on the distribution of forcing events, it is reasonable to assume an increase in event frequency with decreasing ice thickness. The second part of the feedback cycle (Fig. 14 dark green) describes how more deformation events can increase ice thickness through dynamic thickness change. This relationship is less straightforward because thickness change also scales with initial ice thickness. An increase in dynamic thickness change is therefore expressed relative to the initial ice thickness and does not necessarily imply a larger absolute change as the ice thins. We therefore assess whether dynamic thickness change in the Arctic increases with more frequent deformation events or decreases with potentially reduced initial ice thickness.

https://doi.org/10.5194/egusphere-2026-3122
Preprint. Discussion started: 11 June 2026
© Author(s) 2026. CC BY 4.0 License.

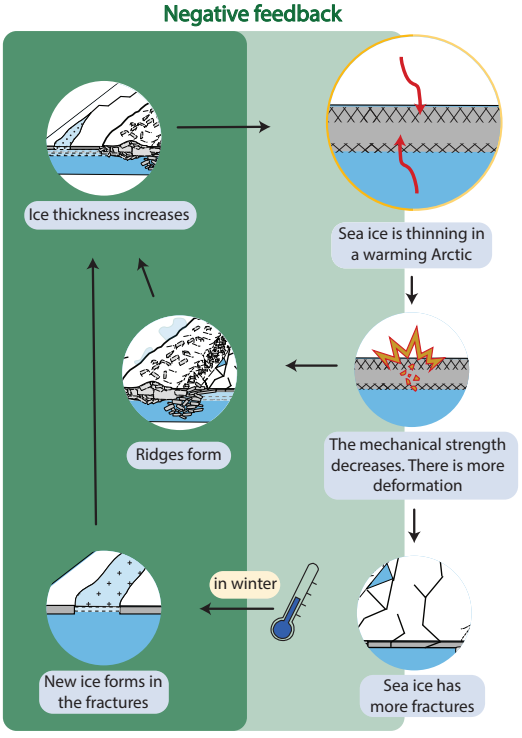


Figure 14. Schematic drawing of the negative winter dynamic thickness feedback associated with sea ice dynamics. The "upward" loop (darker green) of thicker sea ice due to more new ice formation in fractures and ridge formation is discussed here.

We find evidence for the influence of initial ice thickness and deformation on different temporal and spatial scales. At the trajectory scale, dynamic thickness change depends more strongly on initial ice thickness than on deformation, both in observations and simulations. This is evident in the seasonal cycle, where dynamic thickness change peaks later in the season, once the ice is sufficiently thick, rather than in October–November when deformation rates are highest. A similar relationship emerges in the model across thickness classes, with larger changes for thicker ice, and is also evident in the DA-SIT observations, which show a weak positive dependence of thickness change on initial ice thickness (Fig. 13a). In contrast, the correlation between accumulated monthly deformation and dynamic thickness change (DA-SIT$_{\mathrm{dyn}}$) is weak at the trajectory level, likely due to the low signal-to-noise ratio of the deformation forcing.

At the pan-Arctic scale and over long timescales, we observe increases in both net dynamic thickness change (12% per season) and accumulated monthly deformation (1.5% per season). Linear attribution of the dynamic thickness trend shows that it is well explained primarily by increasing deformation (~71%), whereas changes in initial ice thickness contribute negligibly (~2%). In contrast, neither deformation nor thickness explains the (de-trended) interannual variability of the dynamic thickness change at the pan-Arctic scale, suggesting that year-to-year fluctuations are controlled by a non-linear combination of the processes.

https://doi.org/10.5194/egusphere-2026-3122
Preprint. Discussion started: 11 June 2026
© Author(s) 2026. CC BY 4.0 License.

Because intra-seasonal thickness changes are expected to be less affected by sensor-specific uncertainties, we in general consider the trend estimates in DA-SIT$_{\mathrm{dyn}}$ to be robust. However, we also acknowledge that the trend could be influenced by systematic differences in the altimeters. To estimate a potential influence, we consider each altimeter separately, which yields positive, but insignificant trends in both periods, in particular for CryoSat-2. We further note that the remaining differences in the overlapping years are partly an artefact of the curated dataset as the full dataset shows negligible differences between them. Extending the time series towards recent years will help to judge whether the increase that happened particularly after 2013/2014 continues. The consistency of the positive trends across the two independent observational datasets, DA-SIT thickness change and PMW deformation, supports again the robustness of our conclusions: Despite substantial noise, particularly at the trajectory scale, and large intraseasonal variability, those results support the second part of the feedback loop, namely that increased deformation is associated with increased dynamic thickness change.

Our dataset and study setup do not allow us to assess the first part of the feedback loop, i.e. whether thinner ice has caused the increase in deformation (Fig. 14 light green). The ice-thickness trend is uncertain and the deformation record is noisy, so the cause of the observed increase in deformation remains unresolved. It may reflect changes in drift speed associated with atmospheric circulation, i.e., like an observed increase in Arctic cyclone activity (Zhang et al., 2023), reduced ice strength in thinner ice, or a combination of both. Some indications nevertheless point towards thinner ice as a contributing factor. The largest absolute deformation trends occur in early winter, when the strongest thickness changes are also observed (time: 1994–2023 Bocquet et al., 2024), although this is also the season of highest deformation rates. A more conclusive assessment would require robust trends in the frequency and magnitude of deformation events, which cannot be determined using the current dataset. This issue must therefore be addressed in future studies.

Our finding of increasing deformation rates between 2002 and 2020 extends and supports earlier studies reporting rising Arctic deformation activity (Rampal et al., 2009; Krumpen et al., 2025). Given that Krumpen et al. (2025) and Kwok (2006) showed that most ridging events occur in first year ice and become less frequent in multi-year ice, the positive deformation trend is consistent with the transition of the Arctic from a perennial to a more seasonal sea ice cover. The incomplete regional coverage, particularly of regions that experienced a significant decrease in the multi-year ice fraction, prevents a full assessment of this hypothesis. However, the regional deformation trends in Fig. 10a, although not statistically significant, are consistent with this interpretation: strong positive trends in the Beaufort Gyre, where multi-year ice fraction declined strongly, slightly negative trends near Greenland, where multi-year ice fraction remained relatively constant, and no or slightly negative trends across large parts of the Transpolar Drift, where first-year ice fractions were already high after 2010 (e.g., Figure 4 in Kwok, 2018).

An increase in pan-Arctic deformation and dynamic thickness change does not necessarily imply an increase in the total dynamic contribution over the full lifetime of an ice floe. While this may seem counterintuitive, it is consistent with previous studies showing that sea ice age is a key control on surface roughness and dynamic thickness (Krumpen et al., 2025; Sumata et al., 2023; Duncan and Farrell, 2022). Since our analysis focuses on processes within a single season, it does not account for the substantial decrease in Arctic ice residence time (Krumpen et al., 2025; Sumata et al., 2023). Therefore, there is no contradiction: the total contribution of dynamic events to the sea ice thickness has decreased because ice is younger, contribut-

https://doi.org/10.5194/egusphere-2026-3122
Preprint. Discussion started: 11 June 2026
© Author(s) 2026. CC BY 4.0 License.

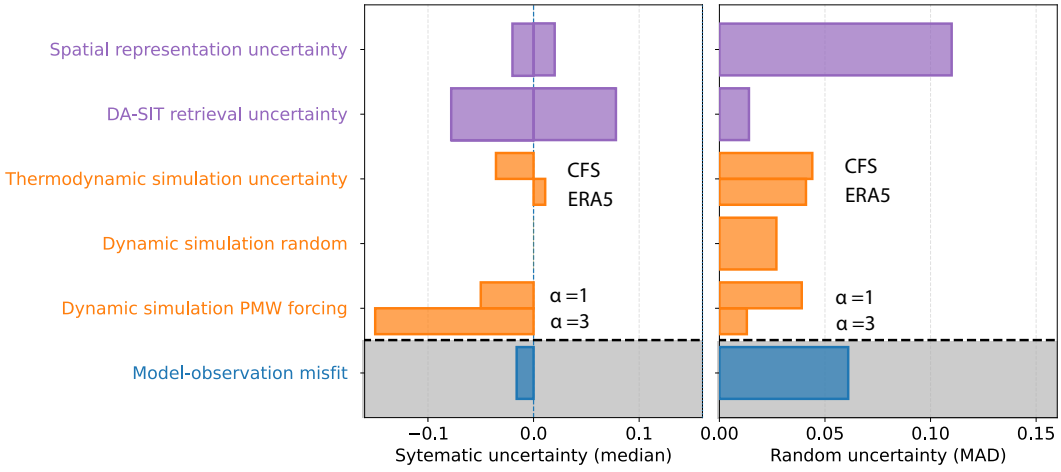


Figure 15. Overview of the main uncertainties related to monthly thickness change, separated into observations (purple) and simulations (orange). The model-observation misfit is displayed in blue. Systematic uncertainty (left) is expressed as the median and random uncertainty (right) is expressed as MAD. For the deformation forcing (RGPS–PMW comparison) two different scaling factors $\alpha = 1$ and $\alpha = 3$ are given.

ing to a thinner and smoother ice cover. Our result adds that, on pan-Arctic scales, dynamic thickness change within a single winter season has also increased. Furthermore, our results qualitatively indicate that the effectiveness of the dynamic thickness feedback weakens for thinner ice (see Fig. 13), raising questions about its future relevance.

We also briefly consider the thermodynamic contribution here. In the Icepack simulations, winter thermodynamic growth changes little over time, except in a few exceptional years. The main peaks follow summers with particularly strong sea-ice loss, notably 2007 and 2012, although the 1-year-delayed response in 2013/2014 remains unresolved. However, our analysis is limited to ice thick enough to be detected by the altimeters and therefore excludes very thin ice and growth from open water. This likely obscures the negative winter growth feedback and complicates the comparison to other studies (e.g., Stroeve et al., 2018).

Overall, the results suggest that increasing deformation in the Arctic has enhanced dynamic thickness change, thereby strengthening winter thickness growth and acting as a negative feedback in the pan-Arctic winter thickness budget. Consequently, the amplitude of winter thickness change increases slightly due to dynamics, implying a stronger seasonal recovery of ice thickness and potentially contributing to the absence of a clear thickness trend despite ongoing warming. At the same time, this feedback is constrained: although dynamic thickness change currently enhances winter recovery, its absolute contribution remains limited by initial ice thickness and may diminish as the ice continues to thin due to climate change.

https://doi.org/10.5194/egusphere-2026-3122
Preprint. Discussion started: 11 June 2026
© Author(s) 2026. CC BY 4.0 License.

5.3 Uncertainties and limitations of the results

The choice of forcing, observational reference data, model configuration, and quality control procedures introduces uncertainties and limitations that constrain the interpretation of the results. These limitations are discussed in the following.

As outlined in Section 4.3, the median of the model-observation misfit is small (8% of the mean monthly thickness change), while the MAD is large (29% of the mean monthly thickness change). This indicates that, on average, the simulations reproduce the observed thickness evolution well, but deviations for individual trajectories can be substantial. The identified uncertainties contribute in different ways to this "total uncertainty". For a better overview of their magnitudes, Figure 15 displays the systematic and random components of the uncertainties along with the "total uncertainty" given by the model-observation misfit.

Systematic uncertainties arise primarily from the simulation framework, in particular from the deformation forcing and its translation into dynamic thickness change (Figure 15). That is well reflected in the clear dependency of the model–observation misfit on the dynamic regime: Icepack underestimates large dynamic thickness changes while overestimating small ones. The comparison to the RGPS data found a systematic underestimation of the total deformation of 30% of the deformation magnitude, which most likely explains a substantial part of the observed median difference in the monthly thickness change which can be up to 60% of the thickness change. Another considerable source is the systematic uncertainty coming from the thickness retrieval. While not discussed in this study, validation exercises on much higher spatial resolution of altimeter-derived thicknesses with independent observations point to an increasing underestimation of thicker ice classes (Paul et al., 2018; Khvorostovsky et al., 2020; Ricker et al., 2025a). Therefore, we speculate that part of the systematic uncertainty of the deformation forcing and thickness retrieval cancel each other. The median difference from the thermodynamic simulations is small and below the individual uncertainty of the IMB measurements. Nevertheless, it is interesting to note that Icepack (forced with ERA5 and CFS-R/v2) overestimates total ice thickness despite also overestimating snow thickness. This may point to issues in the model physics, e.g., too strong thermodynamic growth due to, e.g. an overly high snow conductivity, which is compensated by the too thick snow. As ERA5 is known to have a warm bias, it is unlikely that the overestimation comes from the atmospheric forcing data. The too strong thermodynamic growth could also explain why ERA5 (more snow) outperforms CFS-R/v2 in the comparison of sea ice thickness. However, this effect seems to be most relevant in the beginning of the growth season as for the monthly thickness change (all months equally relevant) of Icepack + ERA5 is slightly positively biased, indicating an underestimation of the change by the simulations.

The dominant contributor to the random uncertainty originates from the observational side (Figure 15). The representation uncertainty alone can explain the observed spread in the model-observation misfit. In addition, uncertainties in the thermodynamic simulations contribute substantially. Spatial misalignment in the deformation forcing ("Dynamic simulation random") plays a comparatively minor role, but the MAD of the RGPS-PMW comparison indicated that there is an additional random uncertainty component in the PMW forcing data that the deformation ensemble runs could not consider.

What does this mean for the robustness of the relative split between the contributions? Icepack appears to slightly overestimate the contribution of dynamics on average, but likely underestimates it in dynamically active regions and seasons, such

https://doi.org/10.5194/egusphere-2026-3122
Preprint. Discussion started: 11 June 2026
© Author(s) 2026. CC BY 4.0 License.

as the convergence and export zones of the Transpolar Drift in autumn. As a consequence, the simulated contrast between dynamically quiet and active regimes is likely weaker than in reality. Despite this limitation, the framework provides a robust basis for pan-Arctic, long-term assessments of dynamic contributions. The availability of observations is a particular advantage compared to other studies, as they allow us to quantify uncertainties and processes separately, and perform quality control measures. However, analyses on the level of individual trajectories remain subject to considerable uncertainty unless additional observational constraints or improved deformation forcing are available.

Beyond these quantified uncertainties, several structural limitations of the study design should be noted.

1. The spatial and temporal resolution of both deformation and thickness data does not allow us to resolve the highly intermittent and localized nature of sea-ice deformation. Instead, the results represent spatially and temporally averaged signals. Differences in scale dependencies between thickness and deformation may introduce an additional bias that is not resolved here.

2. The spatial and temporal variability of thermodynamic growth can only be as realistic as the atmospheric (ERA5 reanalysis) and oceanic (FESOM2 simulation) forcing. Although ERA5 is considered one of the most realistic reanalyses, it is known to have a bias in near-surface temperature. However, validating it in high latitudes is extremely challenging due to the limited number of in situ observations. The oceanic forcing used for the Icepack simulation stems from an ERA5-driven FESOM2 simulation. Vertical mixing in ocean models is still an active field of research and is also very challenging to validate across the entire Arctic. This may affect the representation of basal growth and melt processes, and to a lesser extent, the partitioning between thermodynamic and dynamic contributions.

3. The observational dataset is limited to growth seasons and to ice that is sufficiently thick to be detected by the altimeters. As a result, newly formed and very thin ice are underrepresented. Thus, the relevance of the processes presented here is limited to existing ice, with less weight given to, e.g., the negative winter growth feedback mechanism (e.g., Stroeve et al., 2018). In addition, only ice that is present at the end of spring (April 30) is backtracked; thus, loss of ice before that, i.e. export out of the Arctic or melt, is not included in the analysis. Furthermore, the polar data gap of the two satellite altimeters reduces the spatial coverage. This is particularly relevant during the Envisat period that misses trends closer to the Greenlandic coast to the North Pole where a significant decrease in multi-year ice between 2000 and 2008 occurred (Kwok, 2018). Finally, there is no memory of the ice age or history into the next winter season and all changes happening in summer are not noted, either.

Taken together, these limitations highlight that while the presented framework is well suited for taking stock of the winter sea ice thickness budget on large-scale, long-term scales, caution is required when interpreting individual trajectories. Results are not valid in summer and they do not describe the accumulated effects of thermodynamics and dynamical thickening over several years of growth and melt.

https://doi.org/10.5194/egusphere-2026-3122
Preprint. Discussion started: 11 June 2026
© Author(s) 2026. CC BY 4.0 License.

6 Conclusions and Outlook

We quantify thermodynamic and dynamic contributions to Arctic sea-ice thickness change along trajectories for winters in the period 2002–2020. This is achieved by combining satellite-derived thickness (Envisat, CryoSat-2) with passive-microwave drift and deformation data and Icepack simulations. The approach resolves the individual contributions to the thickness budget and their uncertainties on monthly timescales and $\sim 500\,\mathrm{km} \times 500\,\mathrm{km}$ spatial scales.

Our main finding is that a small pan-Arctic net dynamic contribution to the overall change of 0.21 m per month (Icepack simulations) does not indicate weak dynamics. Instead, strong but opposing processes largely cancel: dynamical thickening (30%) and lead ice growth (10.2%) are balanced by dynamical thinning ($-24\,\%$), alongside thermodynamic growth (35.8%). We show that dynamic thickness change is substantial even in regimes thought to be dynamically quiet. Regional, seasonal, and thickness-dependent variability of the contributions is consistent with large-scale dynamic patterns and physically plausible. The resolved budget components provide a useful framework for diagnosing systematic differences in sea-ice thickness in models, whether sea-ice-only or climate models, as mismatches can be traced back to specific physical processes rather than bulk changes. The sizable role of dynamics also highlights its control on the ice topography, with implications for drag, drift, air–ocean exchange in leads, melt pond evolution, snow redistribution, and ecosystem structure. Future studies could build on this by analyzing dynamic and thermodynamic changes across the full ice thickness distribution and relating their consequences to atmospheric, oceanic, and ecological processes.

Within the limits of the observational datasets, we detect a weak increase in deformation (1.5% per season) and dynamic thickness change (12% per season) on pan-Arctic scales for 2002–2020. These trends provide evidence for part of a negative winter dynamic thickness feedback: enhanced deformation leads to increased dynamical thickening, which partly offsets (summer) sea ice thinning. We note that because this analysis tracks contributions to a single growth season, it does not capture the reduced residence time of Arctic sea ice. Thus, increasing wintertime dynamical thickening coexist with a thinner and younger ice cover (compared to the pre-1990 submarine period, Kwok, 2018), in which the total (accumulated over several years) contribution from dynamics is reduced.

The study design is restricted to sufficiently thick ice, underrepresenting thin and newly formed ice which is most likely why we do not detect a long-term increase in thermodynamic sea ice growth (expected winter sea ice growth feedback). Further, only ice surviving until late spring is tracked, excluding earlier export or melt, making it difficult to compare to Eulerian studies with flux gate approaches. Spatial coverage is further limited by the polar data gap, particularly during the Envisat period. We acknowledge that our results represent spatial and temporal averages that cannot resolve individual deformation processes but only their accumulated effects. Quantifying uncertainties, we note a small bias but a large spread indicating that, on average, the contributions derived from the Icepack simulations reproduce the observed thickness evolution well, but deviations for individual trajectories can be substantial. Systematic uncertainties arise from smoothed deformation forcing, which likely dampens strong events and exaggerates weak ones, limiting the representation of localized and intermittent deformation.

This study cannot address whether thinner ice promotes increased deformation, as this would require robust long-term trends in both the frequency and magnitude of deformation events. Progress in this direction depends on consistent, pan-Arctic, high-

https://doi.org/10.5194/egusphere-2026-3122
Preprint. Discussion started: 11 June 2026
© Author(s) 2026. CC BY 4.0 License.

resolution deformation datasets, for example from SAR-based products (Plante et al., 2025), which can better resolve the intermittent and localized nature of sea-ice deformation. Improved observations of sea-ice thickness are equally critical. A promising approach for connecting thickness change and deformation at higher spatial resolution is using data from the laser altimeter ICESat-2 which is capable of resolving individual ridges (e.g., Farrell et al., 2020; Duncan and Farrell, 2022). The upcoming Copernicus Polar Ice and Snow Topography Altimeter (CRISTAL), planned for launch in 2027, represents a major step forward in reducing the sea ice thickness retrieval uncertainties (Kern et al., 2020). The measurement set-up of CRISTAL is expected to retrieve simultaneously sea-ice freeboard and overlying snow depth at higher along-track resolution (80 m instead of 300 m for CryoSat-2 and potentially $\sim$1 m with fully focused processing) which will open new opportunities to resolve trends in thickness and to better link deformation and thickness changes across scales, especially if better retrieval algorithms can be transferred to older radar altimeters.

Finally, the process-level understanding developed here paves the way for more targeted model evaluation as the explicit separation of thermodynamic and dynamic contributions allows to systematically attribute model biases to specific processes. As Icepack/CICE is widely used in climate models, the insights gained here could be useful for improving the representation of sea-ice dynamics in these systems.

Data availability.

- The DA-SIT customized version with trajectories backtracked from April 30 to October 1 and with a spatial resolution of 75 km is available from Zenodo: https://doi.org/10.5281/zenodo.20117910 (Ricker and von Albedyll, 2026)
- Trajectories with sea ice thickness, deformation, and Icepack simulations are available from Zenodo: 10.5281/zenodo.20036818 (von Albedyll et al., 2026)
- IMB buoys hosted on the Sea Ice Portal are published with uncertainty estimates on Pangaea: https://doi.pangaea.de/10.1594/PANGAEA.973193 (Preußer et al., 2025) (last access: 11 September 2024)
- IMB buoys hosted on the CRREL-Dartmouth Mass Balance Buoy Program can be obtained from http://imb-crrel-dartmouth.org (Perovich et al., 2024) (last access: 5 June 2024)
- The DA-SIT data record (v100) is available on Zenodo: https://doi.org/10.5281/zenodo.14733132 (Ricker et al., 2025b)
- Sea ice drift (https://doi.org/10.15770/EUM_SAF_OSI_0012, (EUMETSAT OSI SAF, 2022b)) and concentration (https://doi.org/10.15770/EUM_SAF_OSI_0013, (EUMETSAT OSI SAF, 2022a)) were obtained from ftp://osisaf.met.no (last access: 20 January 2025).
- Icepack 1.1.0 can be obtained from Zenodo: https://doi.org/10.5281/zenodo.1890602 (Hunke et al., 2018).
- Pre-processed RGPS data is available on Zenodo: https://doi.org/10.5281/zenodo.6321327 (Bouchat and Hutter, 2022)

https://doi.org/10.5194/egusphere-2026-3122
Preprint. Discussion started: 11 June 2026
© Author(s) 2026. CC BY 4.0 License.

- The hourly ERA5 reanalysis is mirrored at the German Climate Computing Center, from where it was downloaded. Access is restricted.
- The 6-hourly NCEP Climate Forecast System Reanalysis (CFSR) (Saha et al., 2010) and the NCEP Climate Forecast System Version 2 (CFSv2) (Saha et al., 2014) were downloaded from https://gdex.ucar.edu/datasets/d093000/dataaccess and https://gdex.ucar.edu/datasets/d094000, respectively.

Author contributions.

Original idea: LvA, SH. Icepack simulations: LvA, FK, DK. Sea ice thickness data input and interpretation: RR, SH, LvA. Algorithm development and analysis: LvA. Discussion of results and conclusions: all authors. Writing the paper: all authors.

Competing interests.

Acknowledgements. This work was funded by a European Space Agency Climate Change Initiative Research Fellowship awarded to LvA (ACCURATE, contract number 4000142016/23/I/DT-lr). RR and SH acknowledge support from the ESA CCI Sea Ice project (CCN-2 and CCN-5 to Contract No. 4000126449/19/I-NB – Sea_Ice_cci) and RR from the Fram Centre project "Sustainable Development of the Arctic Ocean" (SUDARCO, project_ID: 2551323). DK was funded by the CryoSat-2 ThEMatic PrOducts | Cryo-TEMPO project (ESA Contract No. 4000132237/21/I-NS, Phase 3). AI tools (ChatGPT, DeepL, Claude) were used to assist in questions of language and code review. The authors thank Nils Hutter and Christian Haas for advice and fruitful discussions and David Clemens-Sewall and Madison Smith for valuable support in designing the project.

7 Appendix

7.1 Choice of Icepack set-up

7.1.1 Thermodynamics

We tuned the one-step mushy thermodynamics following Plante et al. (2024) using different values for ω (dSdt_slow_mode) and ϕ_{init} (phi_i_mushy). For ω we tested -5.0×10^{-8} m s^{-1}, the default value in Icepack, and -1.5×10^{-7} m s^{-1}, the value suggested in the Icepack documentation. For ϕ_{init} we considered 0.25, 0.45, which was identified as optimal in Plante et al. (2024), 0.65, and 0.85, the default in Icepack. Figure 16 presents a heatmap of the different setups based on daily thickness differences between the IMBs and Icepack simulations (6330 observations) and monthly thickness change differences (5146 observations).

https://doi.org/10.5194/egusphere-2026-3122
Preprint. Discussion started: 11 June 2026
© Author(s) 2026. CC BY 4.0 License.

The differences between the tuning runs are small, on the order of a few centimeters. Interestingly, daily and monthly evaluations reveal opposing trends. Daily bias and RMSE increase with smaller ω and larger ϕ_{init}. The combination $\omega = -1.5 \times 10^{-7}$ m s^{-1} and $\phi_{init} = 0.25$ yields the smallest daily bias. Overall, Icepack overestimates ice thickness. In contrast, monthly bias decreases with larger ϕ_{init} and smaller ω. The combination $\omega = -5.0 \times 10^{-8}$ m s^{-1} and $\phi_{init} = 0.85$ gives the smallest monthly bias, although the differences are on the order of millimeters and therefore negligible in our case. Icepack overall underestimates thickness change. As this study's focus is on monthly thickness change, we select $\omega = -5.0 \times 10^{-8}$ m s^{-1} and $\phi_{init} = 0.85$ as the final configuration.

Our results show that Icepack overestimates the snow thickness, with a smaller bias ($\pm$ RMSE) in CFS-R/v2-forced simulations of -0.042 ± 0.098 m (full season) and -0.016 ± 0.048 m (monthly change) which is almost half of the bias of ERA5 (-0.080$\pm$0.130 m, full season, -0.027 $\pm$0.055 m monthly change). The spread, expressed in the RMSE, is similar for both forcings (Figure 17a,b).

Contrary to what is expected from the snow overestimation, Icepack also overestimates the ice thickness on average. ERA5 shows a median bias of -0.050 m (MAD: 0.081 m) for the ice thickness and 0.011 m per month (MAD: 0.041 m per month) for the monthly changes (Figure 17d,e). Simulations with CFS-R/v2 show a pronounced difference with a median bias of -0.188 m (MAD: 0.102 m) for the thicknesses and -0.036 m per month (MAD: 0.044 m per month) for the monthly change (Figure 17d,e). We further could exclude a thickness-dependent and regional-dependent bias of the simulations (Figure 17f). Overestimating ice thickness despite overestimating snow thickness may hint to issues in the model physics, e.g., too strong thermodynamic growth, which is compensated by the too thick snow. As ERA5 is known to have a warm bias, it is unlikely that the overestimation comes from the forcing data. The too strong thermodynamic growth could also explain, why ERA5 (more snow) outperforms CFS-R/v2 in the comparison of sea ice thickness.

The comparison with the IMBs showed that Icepack forced with ERA5 simulates thermodynamic thickness change with high accuracy under predominantly growth conditions. Given a mean uncertainty of 0.05 m of the IMBs observations, the remaining difference between Icepack and IMBs which can be fully attributed to the Icepack simulation is negligible.

7.2 Spatial representation uncertainty at different spatial and temporal scales

As discussed in Section 4.3, the spatial representation uncertainty depends on the spatial and temporal scale. We tested different scales to find the one with the smallest uncertainty.

The spatial representation uncertainty decreases with larger scales below the autocorrelation length of sea ice describing different sea ice regimes. Measurement uncertainties related to snow thickness and ice density are also reduced on larger scales smaller than the variability of those properties. In addition, the randomly distributed uncertainties of the sea ice thickness measurements are reduced by averaging over more trajectories.

The study tests different circle radii from 50 to 500 km to select a subset of ice that accurately reflects heterogeneous ice conditions while distinguishing between distinct ice regimes. We aim to find the radius where spatial representativeness is given but different ice regimes are kept separate.

https://doi.org/10.5194/egusphere-2026-3122
Preprint. Discussion started: 11 June 2026
© Author(s) 2026. CC BY 4.0 License.

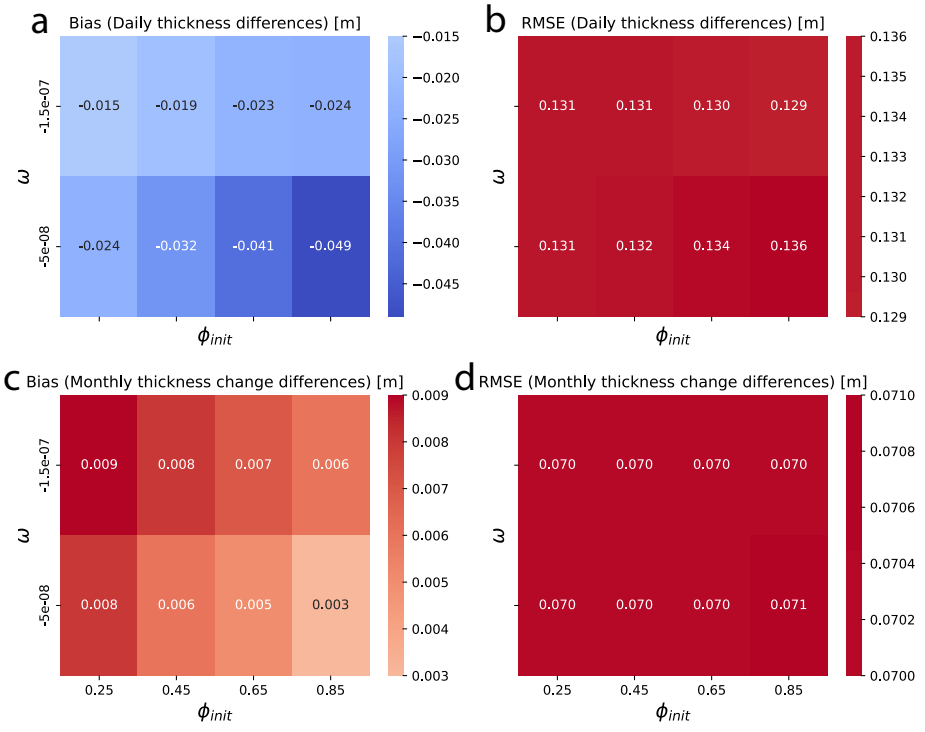


Figure 16. Heatmap of tuning results for ω (dSdt_slow_mode) and ϕ_{init} (phi_i_mushy) in the one-step mushy thermodynamics. Panels a and b show mean (bias) and RMSE of daily thickness differences between IMBs and Icepack simulations, while panels c and d present the corresponding metrics for monthly thickness change differences.

Table 1. Metrics of spatial representation uncertainty on different scales. # points gives the total number of points used in the analysis.

scale	50 km	100 km	200 km	250 km	300 km	350 km	400 km	450 km	500 km
bias [m]	0.01	0.01	0.01	0.01	0.01	0.01	0.01	0.01	0.01
MAD [m]	0.22	0.19	0.23	0.22	0.23	0.24	0.30	0.35	0.32
RMSE [m]	0.32	0.29	0.13	0.13	0.12	0.11	0.13	0.15	0.15
# points	3423	3477	8645	9503	9993	10208	8372	6811	6449

To do so, we analyze the difference between consecutive daily sea ice thickness measurements where regional deformation is minimal (below 1% per day). We calculate the mean of all differences (bias), the mean absolute difference (MAD), and the Root Mean Square Error (RMSE).

Table 1 gives an overview of the day-to-day comparison at different scales. While the different radii do not differ in the bias, the MAD and RMSE are smallest for medium-sized radii. Thus, we select a radius of 250 km for our analysis.

https://doi.org/10.5194/egusphere-2026-3122
Preprint. Discussion started: 11 June 2026
© Author(s) 2026. CC BY 4.0 License.

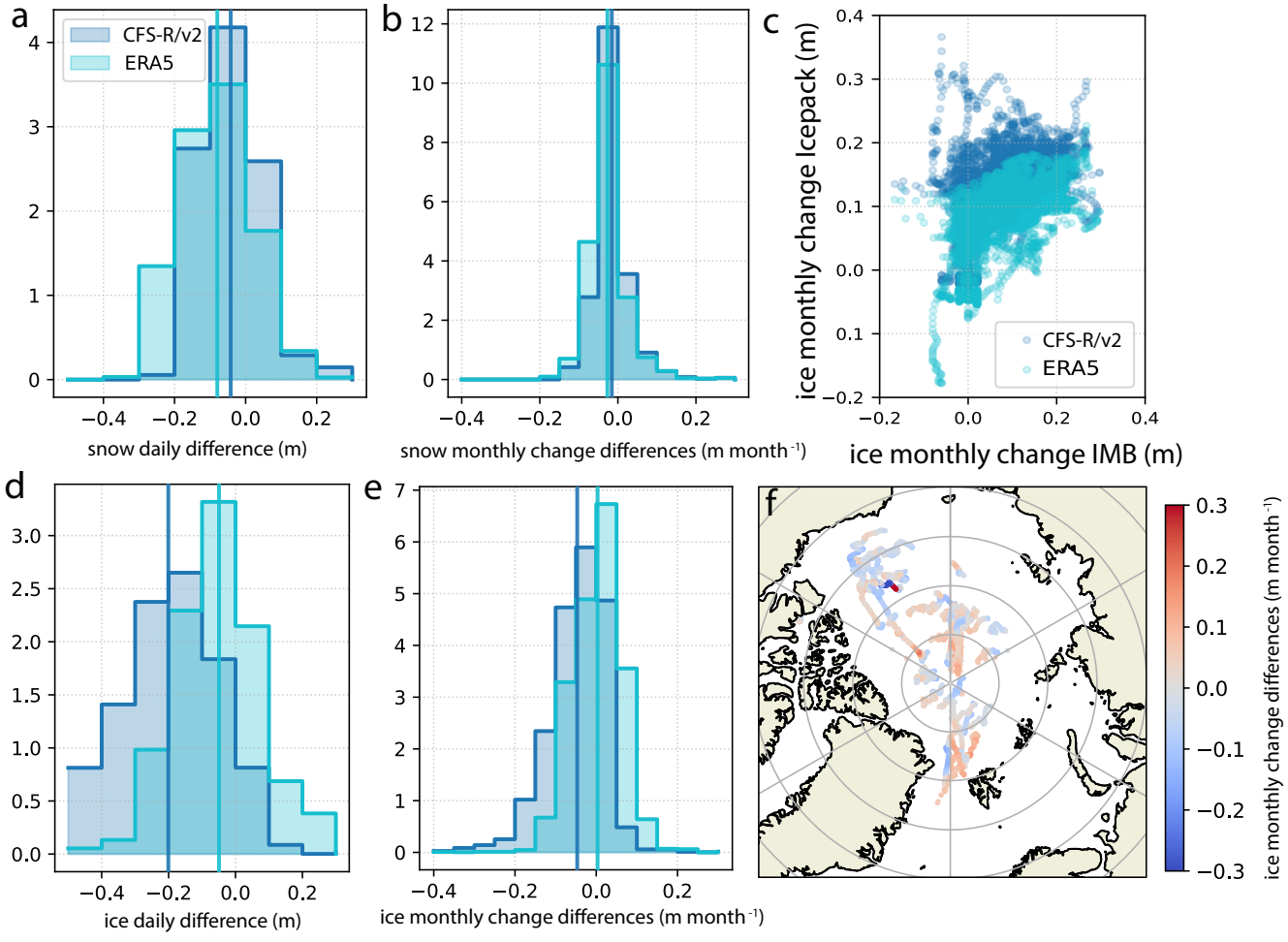


Figure 17. Thermodynamic growth evaluation. Panels a, b, d, and e show probability distribution functions (PDFs) of snow (a, b) and ice thickness (d, e) differences (a, d: daily IMB–Icepack; b, e: monthly change differences, IMB–Icepack) under different atmospheric forcings. Vertical lines indicate the bias of the simulations. Panel c shows the linear relationship and scatter between monthly ice thickness changes from IMBs and the Icepack simulations. Panel f displays the geographic locations where the monthly change differences between IMBs and simulations occur.

https://doi.org/10.5194/egusphere-2026-3122
Preprint. Discussion started: 11 June 2026
© Author(s) 2026. CC BY 4.0 License.

To effectively remove the orbit pattern, we applied a 30-day running mean. To estimate the remaining spatial representation uncertainty, we calculated differences over 30 days to obtain independent observations. Because thermodynamic thickness change cannot be neglected over this period, we subtracted the bias before calculating the MAD and RMSE. We found a bias of 0.16 m, a bias-corrected MAD of 0.11 m, and a bias-corrected RMSE of 0.16 m.

7.3 Constructing polygons from DA-SIT trajectories for deformation estimates

This section aims to give details on how the polygons were constructed from a set of DA-SIT trajectories. For each day, we performed the following steps:

- Collected all available locations for the corresponding day from the set of trajectories ("points").
- Constructed the hull that encloses all points.
- Simplified, if possible, the hull to less than 12 points to reduce computing time.
- Constructed all polygons with a set number of corners based on those simplified hull points. We selected six corner points to decrease the uncertainties (Dierking et al., 2020). In the rare cases when only 4 or 5 points were available, the number of corners was reduced to 4. Below 4 points, no deformation was calculated.
- Selected only polygons without self-intersections, with corner points that are at least 37.5 km apart from each other and with inner angles between 25 and 160 degree.
- Computed the number of points that are enclosed in each polygon and select the 10 polygons with the most enclosed points.
- Calculated deformation for each of the 10 polygons on two different days based on Green's theorem (Kwok et al., 2003, 2008; Dierking et al., 2020). This involves calculating the local velocity field (u,v) from subsequent corner points, calculating strain rates (dudx, dudy, dvdx, dvdy) from the enclosed area (A) and the velocity field, and calculating divergence, shear, and total deformation from the strain rates.
- Averaged the calculated deformation of the 10 polygons (or all, if less than 10 were found) for the respective time step weighted by the number of points they enclose (the more points, the higher the weight).

Our approach produced a time series of mean divergence and shear. As the number of points increases, the polygon's shape approaches a regular hexagon thanks to the weighting scheme. This configuration provides a robust representation of the deformation within the surveyed ice.

In addition, the up to ten daily estimates allow us to quantify the random uncertainty of the deformation forcing related to tracking uncertainties and spatial representation. To estimate its impact on ice thickness, we constructed an ensemble of 1000 realizations for 50 deformation time series (Fig. XX). The ensemble should reproduce the observed mean state, seasonal variability, persistence, and variance structure. Therefore, we build each ensemble from a combination of (a) a nudged

https://doi.org/10.5194/egusphere-2026-3122
Preprint. Discussion started: 11 June 2026
© Author(s) 2026. CC BY 4.0 License.

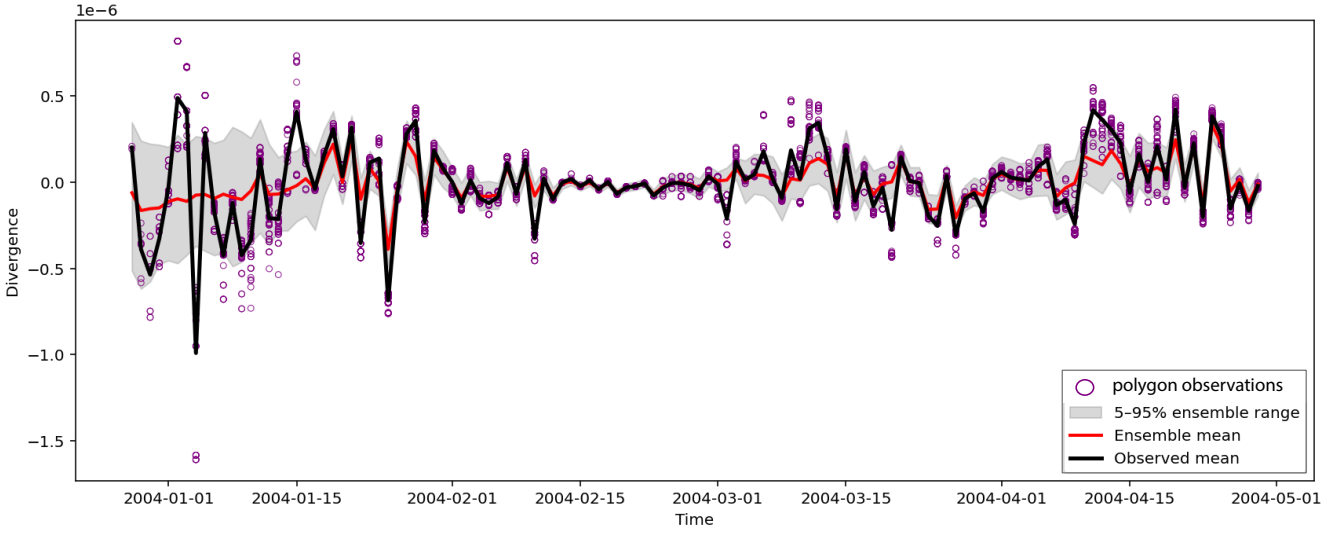


Figure 18. Deformation time series and ensemble. The observed daily mean (black) and ensemble mean (red) are shown together with the 5–95% ensemble range (gray shading) and the individual polygon estimates (purple, up to 10/day). The ensemble spread increases for days with high variance and low sample size. Conversely, for well-constrained days, the ensemble mean transitions from the 30-day running mean toward the observed daily mean.

baseline representing the smoothed large-scale signal and (b) random uncertainty scaled with the variance and spread of the observations.

(a) The 30-day running mean of the observations defines the baseline, which is nudged toward the daily observations depending on their confidence, with higher weight given to days with many polygon estimates and low variance.

(b) On top of this, time-correlated random noise is added using an AR(1) process, with persistence estimated from anomalies relative to the baseline and innovations drawn from a Student-t distribution. The magnitude of this noise is time-dependent and depends on the observational variance and sample size, such that more uncertain days exhibit larger variability. The uncertainty estimates are smoothed over approximately two-week time scales. The AR(1) process introduces temporal persistence, while the heavy-tailed Student-t distribution allows for intermittent large deviations consistent with the observed variability of deformation.

7.4 RGPS-PMW deformation comparison

This section provides details on the comparison of the high-resolution RGPS deformation and low-resolution PMW deformation estimates. For this analysis, we chose a slightly different approach than described before which allows us to compare better temporal variability in deformation across data products. It comes at the cost of characterizing less accurately the deformation within the study area covered by the altimeter observations, which is irrelevant for the comparison. For each polygon, we do the following steps:

https://doi.org/10.5194/egusphere-2026-3122
Preprint. Discussion started: 11 June 2026
© Author(s) 2026. CC BY 4.0 License.

1. We construct the optimal polygon for a set of PMW trajectories (see Section 7.3) at the beginning of the tracking, keep its corner points for all consecutive days, and calculate deformation based on it for each following day. We repeat this procedure for each day (October 1, October 2, ..., April 30) and thus, the number of polygons available for a respective day is increasing.

2. Next, we select all PMW polygons available at the start of the RGPS dataset (January 1 for each year between 2003–2008).

3. For each polygon corner, we search for the RGPS trajectory that is closest, with a maximum distance of 20 km. The selected six RGPS trajectories form the RGPS polygon. While the shape of those polygons is very similar, they are not identical.

4. We calculate deformation from January 1 to March 25 from the RGPS polygons using the same algorithm as for the PMW polygons. Note that the nominal temporal resolution of 3 days of the RGPS trajectories is often not met. We only calculate deformation if two polygons with a 3-day time difference are available, leading to frequent gaps in the RGPS deformation time series.

5. We subset the corresponding PMW polygons to the same temporal resolution as the RGPS polygons (3-daily, with gaps) and calculate deformation based on this reduced dataset.

6. We save each RGPS-PMW deformation pair in containers and average all polygons corresponding to one set of trajectories (“the same ice”) to daily resolution.

For further analysis, we accumulate the daily resolution deformation to monthly aggregates and analyze them as described in Section 4.3.2 (*Uncertainty of the dynamic ice thickness change*). Here, we complement the section with an additional figure on the interannual variability (Figure 19). The matrix of Kolmogorov–Smirnov statistics quantifies similarity (low values) and differences between the datasets in different years. Values along the diagonal represent differences between PMW and RGPS within the same year, while off-diagonal elements indicate interannual differences within each dataset. In general, differences between datasets are comparable to or smaller than differences between years, indicating that PMW captures interannual variability when signals are sufficiently strong, although the signal-to-noise ratio remains limited for weaker variations.

https://doi.org/10.5194/egusphere-2026-3122
Preprint. Discussion started: 11 June 2026
© Author(s) 2026. CC BY 4.0 License.

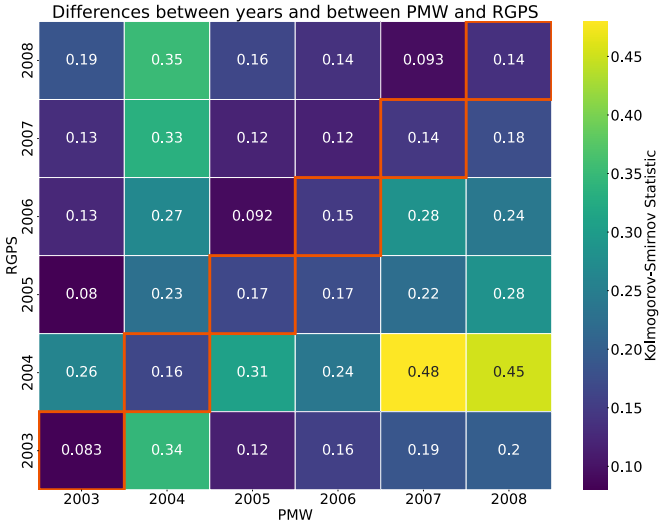


Figure 19. Comparison of interannual variability in accumulated monthly total deformation between RGPS and PMW datasets. Shown are Kolmogorov–Smirnov statistics comparing (i) PMW and RGPS within each year (diagonal), (ii) interannual differences within RGPS (upper triangle), and (iii) interannual differences within PMW (lower triangle).

References

Anheuser, J., Liu, Y., and Key, J. R.: A climatology of thermodynamic vs. dynamic Arctic wintertime sea ice thickness effects during the CryoSat-2 era, The Cryosphere, 17, 2871–2889, https://doi.org/10.5194/tc-17-2871-2023, 2023.

Anheuser, J., Liu, Y., and Key, J.: Model Mean State Sea Ice Thickness Reflects Dynamic Effect Biases: A Process Based Evaluation, Geophysical Research Letters, 51, https://doi.org/10.1029/2023gl106963, 2024.

Bocquet, M., Fleury, S., Rémy, F., and Piras, F.: Arctic and Antarctic Sea Ice Thickness and Volume Changes From Observations Between 1994 and 2023, Journal of Geophysical Research: Oceans, 129, https://doi.org/10.1029/2023jc020848, 2024.

Bouchat, A. and Hutter, N.: Deformation composite of the RADARSAT Geophysical Processor System (RGPS) Lagrangian motion data, https://doi.org/https://doi.org/10.5281/zenodo.6321327, 2022.

Buth, L. G., Krumpen, T., Neckel, N., Webster, M. A., Birnbaum, G., Fuchs, N., Heuser, P., Johannsen, O., and Haas, C.: Characterizing sea ice melt pond fraction and geometry in relation to surface morphology, The Cryosphere, 19, 6527–6545, https://doi.org/10.5194/tc-19-6527-2025, 2025.

Castellani, G., Granskog, M. A., Elias Chereque, A., Chan, A. C. Y., Perez, I., Flores, H., Katlein, C., and Peeken, I.: Arctic sea-ice ridges: a major contributor to algal habitable space in spring, Frontiers in Marine Science, 12, https://doi.org/10.3389/fmars.2025.1653882, 2025.

Clemens-Sewall, D., Polashenski, C., Frey, M. M., Cox, C. J., Granskog, M. A., Macfarlane, A. R., Fons, S. W., Schmale, J., Hutchings, J. K., von Albedyll, L., Arndt, S., Schneebeli, M., and Perovich, D.: Snow Loss Into Leads in Arctic Sea Ice: Minimal in Typical Wintertime Conditions, but High During a Warm and Windy Snowfall Event, Geophysical Research Letters, 50, https://doi.org/10.1029/2023gl102816, 2023.

https://doi.org/10.5194/egusphere-2026-3122
Preprint. Discussion started: 11 June 2026
© Author(s) 2026. CC BY 4.0 License.

Cornish, S. B., Johnson, H. L., Mallett, R. D. C., Dörr, J., Kostov, Y., and Richards, A. E.: Rise and fall of sea ice production in the Arctic Ocean's ice factories, Nature Communications, 13, https://doi.org/10.1038/s41467-022-34785-6, 2022.

Danilov, S., Sidorenko, D., Wang, Q., and Jung, T.: The Finite-volumE Sea ice–Ocean Model (FESOM2), Geoscientific Model Development, 10, 765–789, https://doi.org/10.5194/gmd-10-765-2017, 2017.

Dierking, W., Stern, H. L., and Hutchings, J. K.: Estimating statistical errors in retrievals of ice velocity and deformation parameters from satellite images and buoy arrays, The Cryosphere, 14, 2999–3016, https://doi.org/10.5194/tc-14-2999-2020, 2020.

Duncan, K. and Farrell, S. L.: Determining Variability in Arctic Sea Ice Pressure Ridge Topography With ICESat-2, Geophysical Research Letters, 49, https://doi.org/10.1029/2022gl100272, 2022.

England, M. R., Polvani, L. M., Screen, J., and Chan, A. C.: Minimal Arctic Sea Ice Loss in the Last 20 Years, Consistent With Internal Climate Variability, Geophysical Research Letters, 52, https://doi.org/10.1029/2025GL116175, 2025.

EUMETSAT OSI SAF: OSI-450-a: OSI SAF Global Sea Ice Concentration Climate Data Record 1978–2020 (v3.0), https://doi.org/10.15770/EUM_SAF_OSI_0013, data set, 2022a.

EUMETSAT OSI SAF: OSI-455: OSI SAF Global Low Resolution Sea Ice Drift Data Record 1991–2020 (v1), https://doi.org/10.15770/EUM_SAF_OSI_0012, data set, 2022b.

Farrell, S. L., Duncan, K., Buckley, E. M., Richter-Menge, J., and Li, R.: Mapping Sea Ice Surface Topography in High Fidelity With ICESat-2, Geophysical Research Letters, 47, https://doi.org/10.1029/2020gl090708, 2020.

Fuchs, N., Birnbaum, G., Neckel, N., Kagel, T., Webster, M., and Wernecke, A.: Predicting Melt Pond Coverage on Arctic Sea Ice From Pre-Melt Surface Topography, Geophysical Research Letters, 52, https://doi.org/10.1029/2025gl115033, 2025.

Grosfeld, K., Treffeisen, R., Asseng, J., Bartsch, A., Bräuer, B., Fritzsch, B., Gerdes, R., Hendricks, S., Hiller, W., Heygster, G., Krumpen, T., Lemke, P., Melsheimer, C., Nicolaus, M., Ricker, R., and Weigelt, M.: Online Sea-Ice Knowledge and Data Platform, Polarforschung; 85, https://doi.org/10.2312/POLFOR.2016.011, 2016.

Hendricks, S., Paul, S., and Rinne, E.: ESA Sea Ice Climate Change Initiative (Sea_Ice_cci): Northern hemisphere sea ice thickness from the CryoSat-2 satellite on a monthly grid (L3C), v2.0, https://doi.org/10.5285/FF79D140824F42DD92B204B4F1E9E7C2, 2018a.

Hendricks, S., Paul, S., and Rinne, E.: ESA Sea Ice Climate Change Initiative (Sea_Ice_cci): Northern hemisphere sea ice thickness from the Envisat satellite on a monthly grid (L3C), v2.0, https://doi.org/10.5285/F4C34F4F0F1D4D0DA06D771F6972F180, 2018b.

Heorton, H., Tsamados, M., Landy, J., and Holland, P. R.: Observationally constrained estimates of the annual Arctic sea-ice volume budget 2010–2022, Annals of Glaciology, 66, https://doi.org/10.1017/aog.2025.3, 2025.

Hersbach, H., Bell, B., Berrisford, P., Hirahara, S., Horányi, A., Muñoz-Sabater, J., Nicolas, J., Peubey, C., Radu, R., Schepers, D., Simmons, A., Soci, C., Abdalla, S., Abellan, X., Balsamo, G., Bechtold, P., Biavati, G., Bidlot, J., Bonavita, M., De Chiara, G., Dahlgren, P., Dee, D., Diamantakis, M., Dragani, R., Flemming, J., Forbes, R., Fuentes, M., Geer, A., Haimberger, L., Healy, S., Hogan, R. J., Hólm, E., Janisková, M., Keeley, S., Laloyaux, P., Lopez, P., Lupu, C., Radnoti, G., de Rosnay, P., Rozum, I., Vamborg, F., Villaume, S., and Thépaut, J.: The ERA5 global reanalysis, Quarterly Journal of the Royal Meteorological Society, 146, 1999–2049, https://doi.org/https://doi.org/10.1002/qj.3803, 2020.

Hopkins, M. A.: Four stages of pressure ridging, Journal of Geophysical Research: Oceans, 103, 21 883–21 891, https://doi.org/10.1029/98jc01257, 1998.

Hunke, E., Allard, R., Bailey, D., Blain, P., Craig, T., Damsgaard, A., Dupont, F., DuVivier, A., Grumbine, R., Holland, M., Jeffery, N., Jean-Francois Lemieux, Roberts, A., Turner, M., and Winton, M.: CICE-Consortium/Icepack: Icepack version 1.1.0, https://doi.org/https://doi.org/10.5281/zenodo.1890602, 2018.

https://doi.org/10.5194/egusphere-2026-3122
Preprint. Discussion started: 11 June 2026
© Author(s) 2026. CC BY 4.0 License.

Hunke, E., Allard, R., Bailey, D. A., Blain, P., Craig, A., Dupont, F., DuVivier, A., Grumbine, R., Hebert, D., Holland, M., Jeffery, N., Jean-Francois Lemieux, Osinski, R., Rasmussen, T., Ribergaard, M., Roach, L., Roberts, A., Turner, M., and Winton, M.: CICE-Consortium/Icepack: Icepack 1.2.1, https://doi.org/10.5281/ZENODO.3712299, 2020.

Hutchings, J. K., Roberts, A., Geiger, C. A., and Richter-Menge, J.: Spatial and temporal characterization of sea-ice deformation, Annals of Glaciology, 52, 360–368, https://doi.org/10.3189/172756411795931769, 2011.

Itkin, P. and Liston, G. E.: Combining observational data and numerical models to obtain a seamless high-temporal-resolution seasonal cycle of snow and ice mass balance at the MOSAiC Central Observatory, The Cryosphere, 19, 5111–5133, https://doi.org/10.5194/tc-19-5111-2025, 2025.

Itkin, P., Spreen, G., Cheng, B., Doble, M., Girard-Ardhuin, F., Haapala, J., Hughes, N., Kaleschke, L., Nicolaus, M., and Wilkinson, J.: Thin ice and storms: Sea ice deformation from buoy arrays deployed during N-ICE2015, Journal of Geophysical Research: Oceans, 122, 4661–4674, https://doi.org/10.1002/2016jc012403, 2017.

Itkin, P., Spreen, G., Hvidegaard, S. M., Skourup, H., Wilkinson, J., Gerland, S., and Granskog, M. A.: Contribution of Deformation to Sea Ice Mass Balance: A Case Study From an N-ICE2015 Storm, Geophysical Research Letters, 45, 789–796, https://doi.org/10.1002/2017gl076056, 2018.

Kacimi, S. and Kwok, R.: Arctic Snow Depth, Ice Thickness, and Volume From ICESat-2 and CryoSat-2: 2018–2021, Geophysical Research Letters, 49, https://doi.org/10.1029/2021gl097448, 2022.

Keen, A., Blockley, E., Bailey, D. A., Debernard, J. B., Bushuk, M., Delhaye, S., Docquier, D., Feltham, D., Massonnet, F., O'Farrell, S., Ponsoni, L., Rodriguez, J. M., Schroeder, D., Swart, N., Toyoda, T., Tsujino, H., Vancoppenolle, M., and Wyser, K.: An inter-comparison of the mass budget of the Arctic sea ice in CMIP6 models, The Cryosphere, 15, 951–982, https://doi.org/10.5194/tc-15-951-2021, 2021.

Kern, M., Cullen, R., Berruti, B., Bouffard, J., Casal, T., Drinkwater, M. R., Gabriele, A., Lecuyot, A., Ludwig, M., Midthassel, R., Navas Traver, I., Parrinello, T., Ressler, G., Andersson, E., Martin-Puig, C., Andersen, O., Bartsch, A., Farrell, S., Fleury, S., Gascoin, S., Guillot, A., Humbert, A., Rinne, E., Shepherd, A., van den Broeke, M. R., and Yackel, J.: The Copernicus Polar Ice and Snow Topography Altimeter (CRISTAL) high-priority candidate mission, The Cryosphere, 14, 2235–2251, https://doi.org/10.5194/tc-14-2235-2020, 2020.

Khvorostovsky, K., Hendricks, S., and Rinne, E.: Surface Properties Linked to Retrieval Uncertainty of Satellite Sea-Ice Thickness with Upward-Looking Sonar Measurements, Remote Sensing, 12, 3094, https://doi.org/10.3390/rs12183094, 2020.

Koo, Y., Lei, R., Cheng, Y., Cheng, B., Xie, H., Hoppmann, M., Kurtz, N. T., Ackley, S. F., and Mestas-Nuñez, A. M.: Estimation of thermodynamic and dynamic contributions to sea ice growth in the Central Arctic using ICESat-2 and MOSAiC SIMBA buoy data, Remote Sensing of Environment, 267, 112 730, https://doi.org/10.1016/j.rse.2021.112730, 2021.

Krumpen, T., von Albedyll, L., Bünger, H. J., Castellani, G., Hartmann, J., Helm, V., Hendricks, S., Hutter, N., Landy, J. C., Lisovski, S., Lüpkes, C., Rohde, J., Suhrhoff, M., and Haas, C.: Smoother sea ice with fewer pressure ridges in a more dynamic Arctic, Nature Climate Change, 15, 66–72, https://doi.org/10.1038/s41558-024-02199-5, 2025.

Kwok, R.: Contrasts in sea ice deformation and production in the Arctic seasonal and perennial ice zones, Journal of Geophysical Research, 111, C11S22, https://doi.org/10.1029/2005jc003246, 2006.

Kwok, R.: Arctic sea ice thickness, volume, and multiyear ice coverage: losses and coupled variability (1958–2018), Environmental Research Letters, 13, 105 005, https://doi.org/10.1088/1748-9326/aae3ec, 2018.

Kwok, R. and Cunningham, G. F.: Contributions of growth and deformation to monthly variability in sea ice thickness north of the coasts of Greenland and the Canadian Arctic Archipelago, Geophysical Research Letters, 43, 8097–8105, https://doi.org/10.1002/2016gl069333, 2016.

https://doi.org/10.5194/egusphere-2026-3122
Preprint. Discussion started: 11 June 2026
© Author(s) 2026. CC BY 4.0 License.

Kwok, R., Cunningham, G. F., and Hibler, W. D.: Sub-daily sea ice motion and deformation from RADARSAT observations, Geophysical Research Letters, 30, 2218, https://doi.org/10.1029/2003gl018723, 2003.

Kwok, R., Hunke, E. C., Maslowski, W., Menemenlis, D., and Zhang, J.: Variability of sea ice simulations assessed with RGPS kinematics, Journal of Geophysical Research, 113, https://doi.org/10.1029/2008jc004783, 2008.

Lipscomb, W. H., Hunke, E. C., Maslowski, W., and Jakacki, J.: Ridging, strength, and stability in high-resolution sea ice models, Journal of Geophysical Research, 112, C03S91, https://doi.org/10.1029/2005JC003355, 2007.

Mchedlishvili, A., Lüpkes, C., Petty, A., Tsamados, M., and Spreen, G.: New estimates of pan-Arctic sea ice–atmosphere neutral drag coefficients from ICESat-2 elevation data, The Cryosphere, 17, 4103–4131, https://doi.org/10.5194/tc-17-4103-2023, 2023.

Müller, O., Gardner, J., Olsen, L. M., Salganik, E., Assmy, P., Gradinger, R., Bratbak, G., Hoppe, C. J. M., Lange, B. A., Muilwijk, M., Divine, D. V., Aberle, N., Krause, J. W., Reigstad, M., Leu, E., Tsagaraki, T. M., Larsen, A., Høyland, K. V., Balmonte, J. P., Boulton, W., Dahle, H., Eggers, L., Fong, A. A., Guillou, G., Lebreton, B., Metfies, K., Mock, T., Petelenz, E., Tatarek, A., Torres-Valdés, S., Torstensson, A., Wiktor, J., and Granskog, M. A.: Arctic sea-ice ridges are biomass hotspots harboring diverse microbial communities, Communications Earth amp; Environment, 7, https://doi.org/10.1038/s43247-026-03364-8, 2026.

Nandan, V., Geldsetzer, T., Yackel, J., Mahmud, M., Scharien, R., Howell, S., King, J., Ricker, R., and Else, B.: Effect of Snow Salinity on CryoSat-2 Arctic First-Year Sea Ice Freeboard Measurements, Geophysical Research Letters, 44, https://doi.org/10.1002/2017gl074506, 2017.

Olsen, L. M., Salganik, E., Müller, O., von Albedyll, L., Assmy, P., Granskog, M. A., Hoppe, C. J. M., Campbell, R. G., Larsen, A., Leu, E., Gradinger, R., Gardner, J., Aberle, N., Divine, D. V., Høyland, K. V., Katlein, C., Lange, B. A., Tatarek, A., Wiktor, J., and Bratbak, G.: Sea-ice ridge formation fuels Arctic pelagic food webs during the polar night, Communications Earth amp; Environment, https://doi.org/10.1038/s43247-026-03486-z, 2026.

OSI SAF: Global Sea Ice Drift Climate Data Record Release v1.0 - Multimission, https://doi.org/10.15770/EUM_SAF_OSI_0012, 2022a.

OSI SAF: Global Sea Ice Concentration Climate Data Record v3.0 - Multimission, https://doi.org/10.15770/EUM_SAF_OSI_0013, 2022b.

Paul, S., Hendricks, S., Ricker, R., Kern, S., and Rinne, E.: Empirical parametrization of Envisat freeboard retrieval of Arctic and Antarctic sea ice based on CryoSat-2: progress in the ESA Climate Change Initiative, The Cryosphere, 12, 2437–2460, https://doi.org/10.5194/tc-12-2437-2018, 2018.

Perovich, D., Richter-Menge, J., and Polashenski, C.: Observing and understanding climate change: Monitoring the mass balance, motion, and thickness of Arctic sea ice, http://imb-crrel-dartmouth.org, 2024.

Petrich, C. and Eicken, H.: Overview of Sea Ice Growth and Properties, in: Sea Ice, edited by Thomas, D. N., John Wiley & Sons, Ltd., 3 edn., 2017.

Petty, A. A., Holland, M. M., Bailey, D. A., and Kurtz, N. T.: Warm Arctic, Increased Winter Sea Ice Growth?, Geophysical Research Letters, 45, https://doi.org/10.1029/2018gl079223, 2018.

Plante, M., Lemieux, J.-F., Tremblay, L. B., Tivy, A., Angnatok, J., Roy, F., Smith, G., Dupont, F., and Turner, A. K.: Using Icepack to reproduce ice mass balance buoy observations in landfast ice: improvements from the mushy-layer thermodynamics, The Cryosphere, 18, 1685–1708, https://doi.org/https://doi.org/10.5194/tc-18-1685-2024, 2024.

Plante, M., Lemieux, J.-F., Tremblay, L. B., Bouchat, A., Ringeisen, D., Blain, P., Howell, S., Brady, M., Komarov, A. S., Duval, B., Yakuden, L., and Labelle, F.: A sea ice deformation and rotation rate dataset (2017–2023) from the Environment and Climate Change Canada automated sea ice tracking system (ECCC-ASITS), Earth System Science Data, 17, 423–434, https://doi.org/10.5194/essd-17-423-2025, 2025.

https://doi.org/10.5194/egusphere-2026-3122
Preprint. Discussion started: 11 June 2026
© Author(s) 2026. CC BY 4.0 License.

Polyakov, I. V., Pnyushkov, A. V., Alkire, M. B., Ashik, I. M., Baumann, T. M., Carmack, E. C., Goszczko, I., Guthrie, J., Ivanov, V. V., Kanzow, T., Krishfield, R., Kwok, R., Sundfjord, A., Morison, J., Rember, R., and Yulin, A.: Greater role for Atlantic inflows on sea-ice loss in the Eurasian Basin of the Arctic Ocean, Science, 356, 285–291, https://doi.org/https://doi.org/10.1126/science.aai8204, 2017.

Preußer, A., Nicolaus, M., and Hoppmann, M.: Snow depth, sea ice thickness and interface temperatures derived from measurements of SIMBA buoys deployed in the Arctic Ocean and Southern Ocean between 2012 and 2023, https://doi.org/https://doi.pangaea.de/10.1594/PANGAEA.973193, 2025.

Rampal, P., Weiss, J., and Marsan, D.: Positive trend in the mean speed and deformation rate of Arctic sea ice, 1979–2007, Journal of Geophysical Research, 114, C05 013, https://doi.org/10.1029/2008jc005066, 2009.

Rantanen, M., Karpechko, A. Y., Lipponen, A., Nordling, K., Hyvärinen, O., Ruosteenoja, K., Vihma, T., and Laaksonen, A.: The Arctic has warmed nearly four times faster than the globe since 1979, Communications Earth amp; Environment, 3, https://doi.org/10.1038/s43247-022-00498-3, 2022.

Ricker, R. and von Albedyll, L.: Drift-aware sea ice thickness dataset from satellite remote sensing (trajectories from Oct to Apr and parcel width of 75km), https://doi.org/10.5281/zenodo.20117910, 2026.

Ricker, R., Kauker, F., Schweiger, A., Hendricks, S., Zhang, J., and Paul, S.: Evidence for an increasing role of ocean heat in Arctic winter sea ice growth, Journal of Climate, 34, 5215–5227, https://doi.org/10.1175/jcli-d-20-0848.1, 2021.

Ricker, R., Lavergne, T., Hendricks, S., Paul, S., Down, E., Killie, M. A., and Bocquet, M.: Drift-aware sea ice thickness maps from satellite remote sensing, The Cryosphere, 19, 3785–3803, https://doi.org/10.5194/tc-19-3785-2025, 2025a.

Ricker, R., Lavergne, T., Hendricks, S., Paul, S., Down, E., Killie, M. A., and Bocquet, M.: Drift-aware sea ice thickness maps from satellite remote sensing, https://doi.org/10.5281/ZENODO.14733132, 2025b.

Saha, S., Moorthi, S., Pan, H.-L., Wu, X., Wang, J., Nadiga, S., Tripp, P., Kistler, R., Woollen, J., Behringer, D., Liu, H., Stokes, D., Grumbine, R., Gayno, G., Wang, J., Hou, Y.-T., Chuang, H.-y., Juang, H.-M. H., Sela, J., Iredell, M., Treadon, R., Kleist, D., Van Delst, P., Keyser, D., Derber, J., Ek, M., Meng, J., Wei, H., Yang, R., Lord, S., van den Dool, H., Kumar, A., Wang, W., Long, C., Chelliah, M., Xue, Y., Huang, B., Schemm, J.-K., Ebisuzaki, W., Lin, R., Xie, P., Chen, M., Zhou, S., Higgins, W., Zou, C.-Z., Liu, Q., Chen, Y., Han, Y., Cucurull, L., Reynolds, R. W., Rutledge, G., and Goldberg, M.: The NCEP Climate Forecast System Reanalysis, Bulletin of the American Meteorological Society, 91, 1015–1058, https://doi.org/10.1175/2010bams3001.1, 2010.

Saha, S., Moorthi, S., Wu, X., Wang, J., Nadiga, S., Tripp, P., Behringer, D., Hou, Y.-T., Chuang, H.-y., Iredell, M., Ek, M., Meng, J., Yang, R., Mendez, M. P., van den Dool, H., Zhang, Q., Wang, W., Chen, M., and Becker, E.: The NCEP Climate Forecast System Version 2, Journal of Climate, 27, 2185–2208, https://doi.org/10.1175/jcli-d-12-00823.1, 2014.

Stewart, J. S. and Meier, W. N.: A new regional mask for Arctic sea ice trends and climatologies, NSIDC, https://insidecires.colorado.edu/rendezvous/uploads/Rendezvous_2021_1448_1619668996.pdf, 2021.

Stroeve, J. C., Schroder, D., Tsamados, M., and Feltham, D.: Warm winter, thin ice?, The Cryosphere, 12, 1791–1809, https://doi.org/10.5194/tc-12-1791-2018, 2018.

Sumata, H., de Steur, L., Divine, D. V., Granskog, M. A., and Gerland, S.: Regime shift in Arctic Ocean sea ice thickness, Nature, 615, 443–449, https://doi.org/10.1038/s41586-022-05686-x, 2023.

Ungermann, M. and Losch, M.: An Observationally Based Evaluation of Subgrid Scale Ice Thickness Distributions Simulated in a Large-Scale Sea Ice-Ocean Model of the Arctic Ocean, Journal of Geophysical Research: Oceans, 123, 8052–8067, https://doi.org/10.1029/2018jc014022, 2018.

https://doi.org/10.5194/egusphere-2026-3122
Preprint. Discussion started: 11 June 2026
© Author(s) 2026. CC BY 4.0 License.



von Albedyll, L., Haas, C., and Dierking, W.: Linking sea ice deformation to ice thickness redistribution using high-resolution satellite and airborne observations, The Cryosphere, 15, 2167–2186, https://doi.org/10.5194/tc-15-2167-2021, 2021.

von Albedyll, L., Hendricks, S., Grodofzig, R., Krumpen, T., Arndt, S., Belter, H. J., Birnbaum, G., Cheng, B., Hoppmann, M., Hutchings, J., Itkin, P., Lei, R., Nicolaus, M., Ricker, R., Rohde, J., Suhrhoff, M., Timofeeva, A., Watkins, D., Webster, M., and Haas, C.: Thermodynamic and dynamic contributions to seasonal Arctic sea ice thickness distributions from airborne observations, Elementa: Science of the Anthropocene, 10, https://doi.org/10.1525/elementa.2021.00074, 2022.

von Albedyll, L., Ricker, R., Hendricks, S., Kauker, F., and Krogmann, D.: Trajectories of Arctic sea ice thickness change and its thermodynamic and dynamic contributions (2002–2020), https://doi.org/10.5281/zenodo.20036818, 2026.

Wang, Q., Danilov, S., Sidorenko, D., Timmermann, R., Wekerle, C., Wang, X., Jung, T., and Schröter, J.: The Finite Element Sea Ice-Ocean Model (FESOM) v.1.4: formulation of an ocean general circulation model, Geoscientific Model Development, 7, 663–693, https://doi.org/10.5194/gmd-7-663-2014, 2014.

Willatt, R., Laxon, S., Giles, K., Cullen, R., Haas, C., and Helm, V.: Ku-band radar penetration into snow cover on Arctic sea ice using airborne data, Annals of Glaciology, 52, 197–205, https://doi.org/10.3189/172756411795931589, 2011.

Zhang, X., Tang, H., Zhang, J., Walsh, J. E., Roesler, E. L., Hillman, B., Ballinger, T. J., and Weijer, W.: Arctic cyclones have become more intense and longer-lived over the past seven decades, Communications Earth amp; Environment, 4, https://doi.org/10.1038/s43247-023-01003-0, 2023.